MEASUREMENTS OF THERMALLY ACTIVATED RELAXATION TIMES IN AMORPHOUS POLY(METHYL METHACRYLATE) USING PHOTON CORRELATION SPECTROSCOPY.

by

George Henry Gangwere III

B.S., Southwest Missouri State University, 1977

A Master's Thesis

Submitted in partial fulfillment of the

requirements for the degree

MASTER OF SCIENCE

Department of Physics

Kansas State University
Manhattan, Kansas

1981

Approved by:

Major Professor

THIS BOOK
CONTAINS
NUMEROUS PAGES
WITH THE ORIGINAL
PRINTING BEING
SKEWED
DIFFERENTLY FROM
THE TOP OF THE
PAGE TO THE
BOTTOM.

THIS IS AS RECEIVED
FROM THE
CUSTOMER.

TABLE OF CONTENTS

LIST OF TABLES

LIST OF FIGURES

ACKNOWLEDGMENTS

I want to express my gratitude to my major professor, Chris Sorensen, for his help and guidance in the experimental as well as the writing stages of this thesis. I also want to thank him for his patience and encouragement during the difficult times.

I would like to thank Dr. Compaan for the many helpful comments he gave me in the laboratory.

I would also like to thank both Dr. Compaan and Dr. Spangler for serving on my committee.

Chapter I

INTRODUCTION

1.1 Synopses

Scattering of electromagnetic radiation is an important tool in the study of the structure and dynamics of matter. To name just a few examples, Raman scattering enables us to obtain information about the energy spectra of molecules, x-ray diffraction provides information about the structure of solids, and Brillouin scattering can provide information on sound waves in solids.

Until recently, traditional dispersive or interferometric spectroscopes have been limited to resolving powers of a few MHz. With the advent of the laser and a new kind of spectroscopy, light beating or photon correlation spectroscopy,[1] it is now possible to measure linewidths and frequency shifts of the order of a few Hz. Light-beating spectroscopy has made it possible for chemists, biologists and physicists to study the size, shape and motions of molecules in such diverse systems as solids, glasses, simple molecular fluids, solutions of biological macro-molecules, solutions of viruses, protoplasm in algae, colloidal dispersions and mixtures undergoing critical point fluctuations.

The first application of light-beating spectroscopy came in 1964 when Cummins, et al. studied the spectrum of light scattered from polystyrene latex spheres diffusing in a dilute solution.[2] Other applications were quick to follow. For example, concentration fluctuations which cause

critical opalescence were studied by Alpert, et al. in 1965.[3] In that same year Ford and Benedek studied the scattered light from a fluid near the fluid-vapor critical point.[4] For the interested reader, references five through eight represent some of the early applications of light-beating spectroscopy.

It is the purpose of this thesis is to report the application of light-beating spectroscopy to the study of the spectrum of light scattered from commercial poly(methyl methacrylate) (PMMA). The specific technique used is a digital form of photon correlation spectroscopy.

The remainder of this chapter is devoted to the discussion of the principles of a typical light-beating experiment.

1.2 The Light-Beating Spectrometer

Figure 1.2.1 shows the geometry of a typical light-scattering experiment. Laser light with polarization $\hat{n}_i$ and wave vector $\vec{k}_i$ is focused onto a cell containing the sample. The scattered light with polarization $\hat{n}_s$ and wave vector $\vec{k}_s$ is intercepted by the detector at a distance $\vec{R}$ from the scattering volume. The intersection of the incident beam and the beam collected by the detector defines the scattering volume. The angle between the incident beam and the scattered beam is the scattering angle θ. We define the scattering wave vector $\vec{q}$ as the difference between the scattered and incident wave vectors,

$$\vec{q} = \vec{k}_i - \vec{k}_s \quad . \tag{1.2.1}$$

The magnitude of the scattering vector is given by

$$q = \frac{4\pi n}{\lambda_i} \sin\left[\frac{\theta}{2}\right] \quad , \tag{1.2.2}$$

Figure 1.2.1

Geometry of a typical light-scattering experiment.

THIS BOOK CONTAINS NUMEROUS PAGES WITH DIAGRAMS THAT ARE CROOKED COMPARED TO THE REST OF THE INFORMATION ON THE PAGE.

THIS IS AS RECEIVED FROM CUSTOMER.

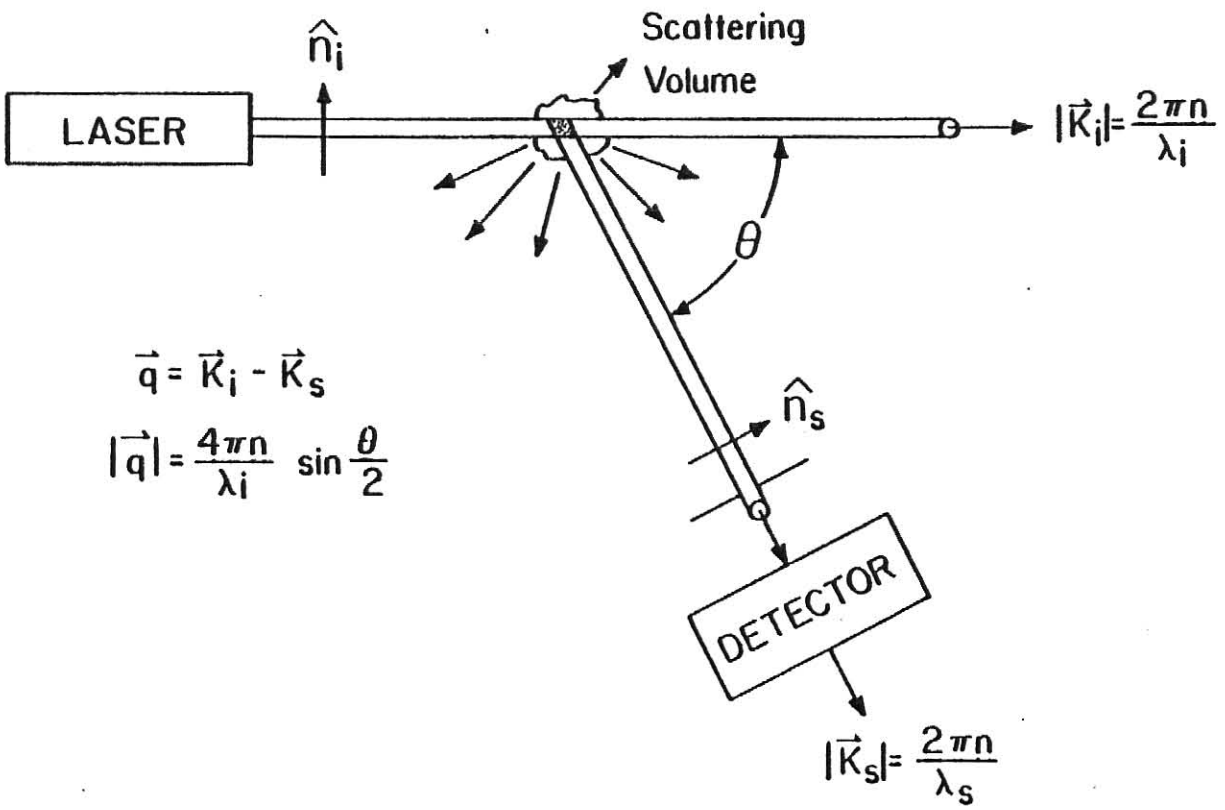
LASER
$\hat{n}_i$
Scattering
Volume
$|\vec{K}_i| = \frac{2\pi n}{\lambda_i}$
θ
$\hat{n}_s$
DETECTOR
$|\vec{K}_s| = \frac{2\pi n}{\lambda_s}$
$\vec{q} = \vec{K}_i - \vec{K}_s$
$|\vec{q}| = \frac{4\pi n}{\lambda_i} \sin\frac{\theta}{2}$

where n is the index of refraction of the scattering medium and λ_i is the wavelength in vacuo of the incident radiation.

Light scattering does not occur in a perfectly uniform, homogeneous material. If scattering is to occur, the local dielectric constant of the medium must be nonuniform. This may be provided by non-propagating thermodynamic fluctuations of the local dielectric constant as a result of the motions of the molecules that constitute the material. Scattering by this process is known as Rayleigh scattering.

The amplitude of the total scattered electric field changes with time since the phase of the field scattered by each molecule relative to the others is also changing with time as the molecules move. The frequency spectrum linewidth of the scattered light depends on the time scales which characterize the motions of the molecules. For time scales normally encountered in glassy polymers, the linewidths are relatively narrow (10^6Hz - 10^{-2}Hz) and are centered about the incident light frequency (~10^{14}Hz). Measurement of these linewidths would require an optical spectrometer with resolving power beyond present capabilities.

An alternate method is photon correlation spectroscopy. Figure 1.2.2 shows pictorially the signal output and the associated power spectrum for the various components of a correlation spectrometer. The incident laser light can be thought of as a monochromatic carrier wave with a frequency of approximately 10^{14}Hz and essentially a delta function profile in frequency space. The scattering process modulates the carrier wave producing a spread of frequencies. The result is a Lorentzian with half-width at half-height Γ. The photomultiplier's response time (~10^{-9}sec)

Figure 1.2.2

Signal output and the associated power spectrum for the various components of a correlation spectrometer. a) Laser carrier wave with frequency ω_0 b) modulation of the carrier wave due to the scattering process, c) the output of the photomultiplier is a series of pulses proportional to the modulation frequency, d) photopulse autocorrelation function, e) delta function power spectrum centered at ω_0, f) spread of frequencies produced by the scattering process and centered at ω_0, g) self-beat power spectrum of width 2Γ centered at 0Hz.

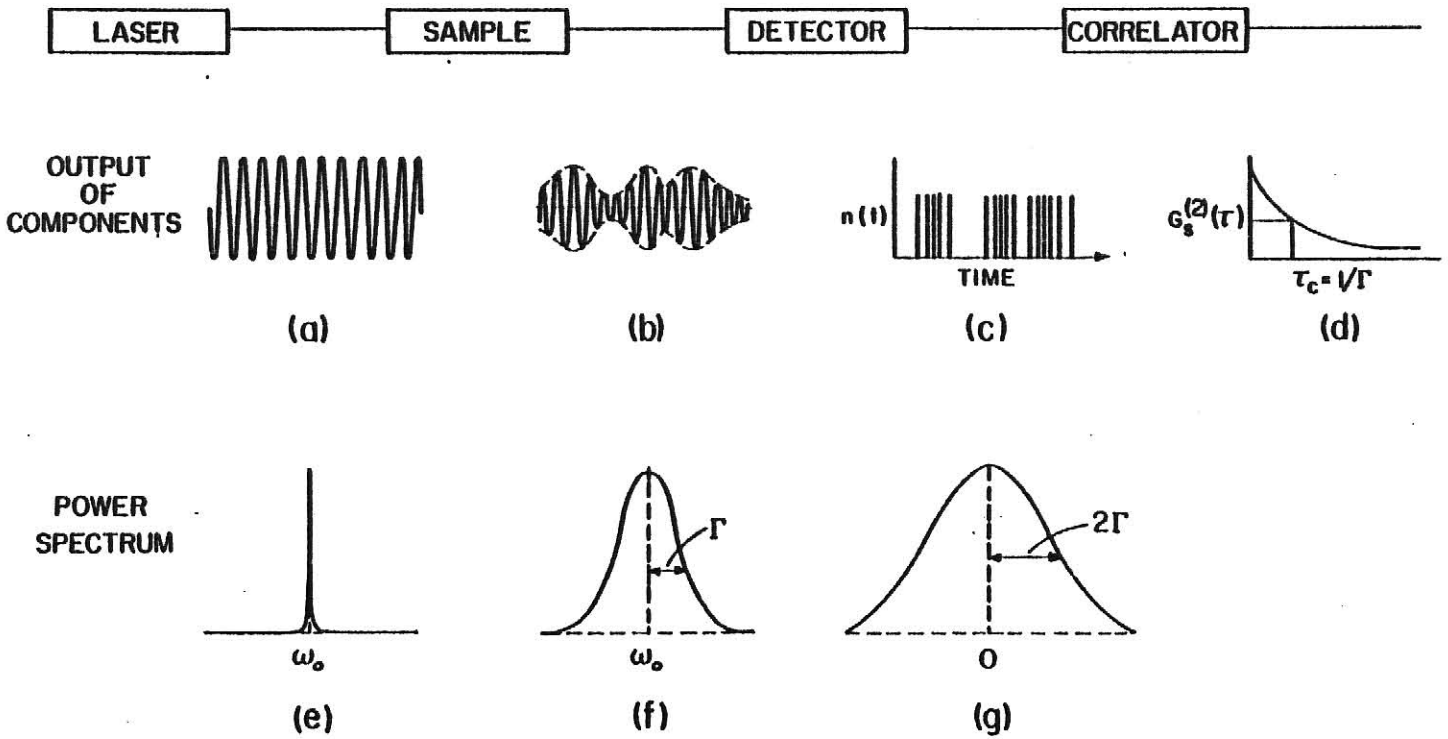
LASER
SAMPLE
DETECTOR
CORRELATOR
OUTPUT OF COMPONENTS
n(t)
TIME
$G_s^{(2)}(\tau)$
$\tau_c = 1/\Gamma$
(a)
(b)
(c)
(d)
POWER SPECTRUM
ω_o
Γ
ω_o
2Γ
0
(e)
(f)
(g)

is too slow for it to follow the carrier wave frequency. Only the beat frequencies produced by all possible pairs of frequencies that make up the scattered spectrum are detected. As a result, the original spectrum is transformed, after detection, to a new spectrum which is twice as broad and is centered at 0Hz. This process, where the scattered light beats with itself, is called homodyne detection.

Homodyne detection is actually a special case of heterodyne detection. Heterodyne detection occurs when the scattered light beats with a local oscillator source derived from the same laser as used for the scattering. The resultant spectrum can be very complicated since the homodyne term is still present. However, if the local oscillator intensity is approximately thirty times that of the scattered light, the homodyne spectrum becomes negligible and the heterodyne spectrum dominates.[9]

The homodyne and heterodyne spectra are encoded in the train of photopulses output by the photomultiplier. Linewidth information can be obtained from these pulses by computing either the photocurrent autocorrelation function (analog method) or the photopulse autocorrelation function (digital method). The exact details by which linewidths can be extracted from the autocorrelation functions are the topics of the following chapters.

Chapter II

THE CORRELATION FUNCTIONS

2.1 Definitions and Properties

Mathematically, the autocorrelation function[11] is defined for A(t) as the time average

$$G(\tau) \equiv \underset{T \to \infty}{\text{Limit}} \frac{1}{2T} \int_{-T}^{T} A(t)A(t+\tau)dt \qquad (2.1.1)$$

where A(t) is an arbitrary function of time and τ is the delay time. The autocorrelation function compares the value of the signal A(t), with the value of that same signal at some later time τ, for all values of t.

We can simplify the above equation slightly if we restrict A(t) to ergodic functions.[13] Ergodicity allows us to equate time averages with ensemble averages, hence

$$G(\tau) = \langle A(t)A(t+\tau)\rangle = \underset{T \to \infty}{\text{Limit}} \frac{1}{2T} \int_{-T}^{T} A(t)A(t+\tau)dt \qquad (2.1.2)$$

where the brackets denote the ensemble average. If we make the further restriction that A(t) is a stationary random function of time, then the value of the correlation function is a function of τ only, so that

$$\langle A(o)A(\tau)\rangle = \langle A(t)A(t+\tau)\rangle \quad . \qquad (2.1.3)$$

In order to obtain a feeling for the behavior of the autocorrelation function, consider Fig. 2.1.1 where a typical random and nonperiodic signal is represented as a function of time. The average value of A(t) is set to zero to simplify the following discussion.

When $\tau = 0$ the product A(0)A(0) will always be non negative and the resultant value of the autocorrelation function will be large

$$\lim_{\tau \to 0} \langle A(0)A(\tau)\rangle = \langle A^2\rangle \quad . \tag{2.1.4}$$

For values of τ larger than zero but smaller than the time it takes for the signal to change its value appreciably, the product will almost always be positive but in some instances negative. As a result concellations will occur in the sum implied by the ensemble average and we would expect the value of the autocorrelation function to be less than when $\tau = 0$. Finally, as τ becomes large, the product $A(0)A(\tau)$ will be positive just as much as it is negative and the autocorrelation function will approach zero.

$$\lim_{\tau \to \infty} \langle A(0)A(\tau)\rangle = \langle A\rangle^2 = 0 \quad . \tag{2.1.5}$$

In general, as τ increases from zero, the value of the autocorrelation function will do one of two things for a random nonperiodic process. The autocorrelation function will remain constant at its maximum value of $\langle A^2\rangle$ for all values of τ, in which case A is a constant of the motion. Or the autocorrelation function will decrease from its maximum value of $\langle A^2\rangle$ to the square of the average value of A, $\langle A\rangle^2$.

In many applications the autocorrelation function decays exponentially[12] so that

Figure 2.1.1

A typical random and nonperiodic signal as a function of time. The average value of <A> is set to zero for convenience.

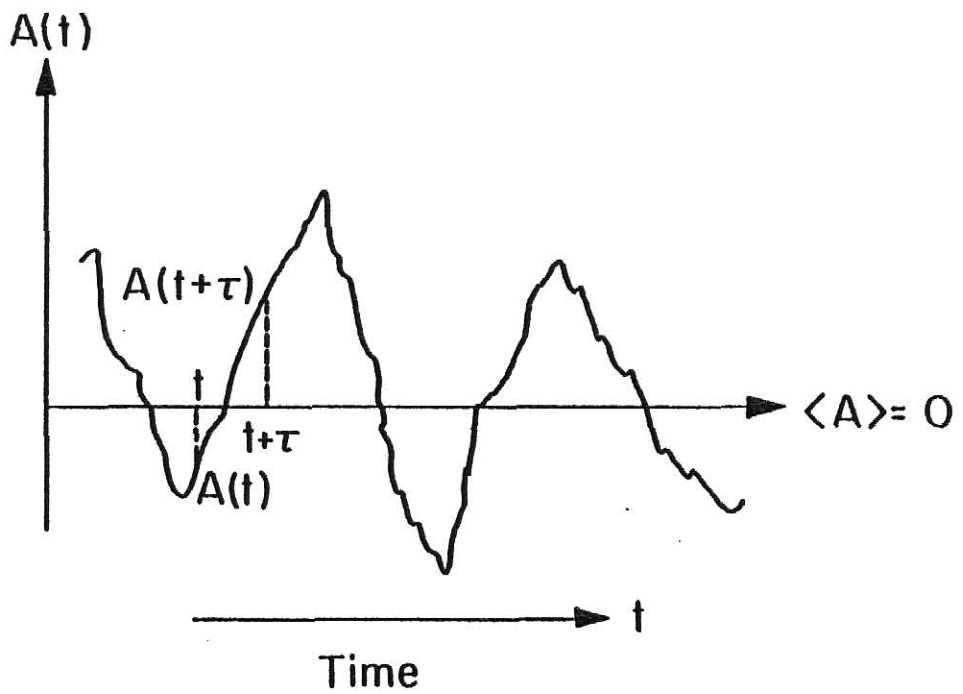
A(t)
A(t+τ)
t
t+τ
A(t)
<A>= 0
t
Time

$$G(\tau) = \langle A \rangle^2 + \{\langle A^2 \rangle - \langle A \rangle^2\} e^{-\tau/\tau_c} \qquad (2.1.6)$$

where τ_c is a characteristic time of the random process, the so-called correlation time.

2.2 The Power Spectrum

The frequency power spectrum and the autocorrelation function are related by the Wiener-Khinchine theorem[14]

$$S(\omega) = \frac{1}{2\pi} \int_{-\infty}^{\infty} G(\tau) e^{i\omega\tau} \, d\tau \quad . \qquad (2.2.1)$$

Thus, the frequency power spectrum and the autocorrelation function are Fourier transform pairs. For example, if the signal A(t) has a Lorentzian power spectrum of half-width at half-height Γ, then $G(\tau)$ is a decaying exponential with correlation time $\tau_c = (\Gamma)^{-1}$.

2.3 First-and Second-Order Electric Field Autocorrelation Functions

We now wish to apply the results discussed in the previous sections to the light-scattering process.

The first-order field autocorrelation function is defined as[15]

$$G_s^{(1)}(\tau) \equiv \langle E_s^*(0) E_s(\tau) \rangle \qquad (2.3.1)$$

where E_s is the scattered electric field[16] and * represents the complex conjugate. It is not possible however, to directly measure $G_s^{(1)}(\tau)$ due to the square-law nature of the detection process. For example, the output of a photomultiplier is proportional to the intensity which is

equal to the square of the scattered electric field. In fact, the lowest-order field autocorrelation function that can be directly measured is the intensity autocorrelation function.

$$G_s^{(2)}(\tau) \equiv \langle I_s(0) I_s(\tau) \rangle \tag{2.3.2}$$

Equations (2.3.1) and (2.3.2) can be written in normalized form

$$g_s^{(1)}(\tau) = \langle E_s^*(0) E_s(\tau) \rangle / \langle I_s \rangle \tag{2.3.3}$$

$$g_s^{(2)}(\tau) = \langle I_s(0) I_s(\tau) \rangle / \langle I_s \rangle^2 \tag{2.3.4}$$

where $\langle I_s \rangle$ is the average intensity over the duration of the experiment.

In certain circumstances, $g_s^{(2)}(\tau)$ can be simply expressed in terms of $g_s^{(1)}(\tau)$. The criteria is that the scattered amplitude, E_s, be distributed according to a Gaussian distribution. We can understand what this means by considering E_s as a superposition of fields scattered from many different regions of the scattering volume,

$$E_s = \sum_{i=1}^{n} E_s^{(i)} \tag{2.3.5}$$

where $E_s^{(i)}$ is the field scattered from the i^{th} region. Each region is taken to be small compared to the wavelength of light yet large enough to enable the molecules in each region to move independently of one another. Under these conditions E_s is the sum of independent random variables. The central limit theorem then implies that E_s must also be a random variable and is distributed according to a Gaussian distribution. That is, the probability that E_s will have a particular value is given by

$$P(E_s) = \frac{1}{\pi \langle |E_s|^2 \rangle} e^{-\frac{|E_s|^2}{\langle |E_s|^2 \rangle}} \quad . \tag{2.3.6}$$

For such a Gaussian field, $g_s^{(2)}(\tau)$ and $g_s^{(1)}(\tau)$ are related in a rather simple manner by the Siegart relation[17]

$$g_s^{(2)}(\tau) = 1 + |g_s^{(1)}(\tau)|^2 \quad . \tag{2.3.7}$$

Thus the Siegart relation enables one to obtain first-order spectral properties from the intensity or second-order autocorrelation function.

We must bear in mind however, that Eq. (2.3.7) applies only to Gaussian fields. If one is unable to invoke Gaussian statistics, first-order spectral properties can still be obtained from the second-order autocorrelation function. This can be achieved by mixing coherently on the sensitive part of the detector the scattered light and a local oscillator source derived from the same laser as used for the scattering. It can then be shown[18] that the measured normalized autocorrelation function takes the form

$$g_{het}^{(2)}(\tau) = 1 + \left(\frac{\langle I_s \rangle}{\langle I \rangle}\right)^2 \left(g_s^{(2)}(\tau) - 1 \right) + 2 \frac{\langle I_s \rangle \langle I_{lo} \rangle}{\langle I \rangle^2} |g_s^{(1)}(\tau)| \tag{2.3.8}$$

where I_s is the intensity due to the scattering process, I_{lo} is the intensity of the local oscillator source and $I(=I_s+I_{lo})$ is the observed total intensity. This type of detection is heterodyne detection as mentioned in Section 1.2.

2.4 The Photopulse Autocorrelation Function

In the digital method the scattered light is detected by a photomultiplier that outputs a train of photoelectron pulses where the pulse rate is proportional to the intensity. These pulses are then amplified and converted to standard (TTL) square pulses. The pulses are then fed into a digital correlator that computes the photopulse autocorrelation function given by

$$G^{(2)}(r\tilde{t}) = \langle n(0)n(r\tilde{t})\rangle \quad , \tag{2.4.1}$$

where $n(r\tilde{t})$ is the number of photopulses arriving during the interval rt to $r(t + \tilde{t})$, $\tilde{t}$ is the sample time[19] and r is the channel number.[20] As long as the correlation function does not change appreciably during the sample time $\tilde{t}$, the discrete function $G^{(2)}(r\tilde{t})$ is a good approximation to the true second-order autocorrelation function $G^{(2)}(\tau)$.

The normalized homodyne and heterodyne autocorrelation functions as computed by the correlator are then

$$g^{(2)}_{hom}(r\tilde{t}) = 1 + |g^{(1)}_s(r\tilde{t})|^2 \tag{2.4.2}$$

$$g^{(2)}_{het}(r\tilde{t}) = 1 + 2\,\frac{\bar{n}_s\bar{n}_{lo}}{\bar{n}^2}\,|g^{(1)}_s(r\tilde{t})| \quad , \quad \bar{n}_{lo} \approx 30\,\bar{n}_s \tag{2.4.3}$$

where $\bar{n}_s$ and $\bar{n}_{lo}$ are the average scattered and local oscillator count-rates respectively, and $\bar{n}$ is the observed average count-rate. (Note that the middle term of Eq. (2.3.8) is negligible when $\bar{n}_{lo} \approx 30\,\bar{n}_s$.)

Chapter III

THE RELAXATION FUNCTION

3.1 Introduction

The purpose of this chapter is to investigate several functional forms that have commonly been used for $|g_s^{(1)}(r\tilde{t})|^{21}$.

Before proceeding, it will be helpful to simplify the notation. One finds that in the literature on glasses the heterodyne and homodyne autocorrelation function are written as follows

$$C_{hom}(t) = 1 + \phi^2(t) \tag{3.1.1}$$

$$C_{het}(t) = 1 + 2\,\frac{\bar{n}_s \bar{n}_{lo}}{\bar{n}^2}\,\phi(t) \qquad , \quad \bar{n}_{lo} \approx 30\,\bar{n}_s \tag{3.1.2}$$

where $\phi(t) \equiv |g_s^{(1)}(r\tilde{t})|$ is commonly referred to as the relaxation function. In addition $C(t) \equiv g^{(2)}(r\tilde{t})$. This will be the notation used throughout the remainder of this report.

It has been shown[12] that for diffusion processes that the relaxation function has the form

$$\phi(t) = e^{-t/\tau_c} \tag{3.1.3}$$

where the correlation time τ_c is referred to as the "relaxation time" of the diffusion process.

Relaxation data for glasses has been obtained chiefly from three

different techniques, mechanical relaxation experiments, dielectric relaxation and photon correlation spectroscopy. Workers using these techniques have discovered that in many different materials including organic liquids[23] and solutions,[24] glass forming materials[25] and polymers,[26] relaxation behavior cannot be expressed as a single exponential parameterized by a single relaxation time. As a result, the data has been fit to two empirical relaxation functions, the Williams-Watts,[27,28] and the Cole-Davidson functions.[29,30] The bulk of the data having been analyzed with the former of these functions.

There are two ways in which physicists have attempted to explain the nonexponential relaxation behavior in materials. One approach interprets the nonexponential behavior as resulting from cooperative molecular motions.[31,32] The other theory sees the nonexponential behavior as due to the superposition of many different exponentially relaxing processes.[33,29] It is not known which one, if either, is the correct theory. However, the current trend is toward the latter approach.

3.2 The Williams-Watts Function

The empirical Williams-Watts relaxation function was first introduced in 1969 and is given by

$$\phi_{WW}(t) = e^{-(t/\tau_{WW})^{\beta_{WW}}} \qquad (3.2.1)$$

where $0<\beta_{WW}\leq 1$. Taking the superposition of exponentials approach, β_{WW} represents the width of the distribution of relaxation times, the width of the distribution increasing with decreasing β_{WW}. We can define the distribution function, $\rho_{WW}(\tau)$, for the Williams-Watts function with the

following equations

$$\phi_{ww}(t) \equiv \int_0^\infty e^{-t/\tau} \rho_{ww}(\tau) d\tau \quad . \tag{3.2.2}$$

and the normalization condition

$$\int_0^\infty \rho_{ww}(\tau) d\tau = 1 \quad . \tag{3.2.3}$$

The average relaxation time is defined by

$$\langle \tau_{ww} \rangle \equiv \int_0^\infty \tau \rho_{ww}(\tau) d\tau \quad . \tag{3.2.4}$$

$\rho_{ww}(\tau)$ has only recently been derived from Eq. (3.2.2)[22] however, the knowledge of $\rho_{ww}(\tau)$ is not needed to determine the average relaxation time. It has been shown that

$$\langle \tau_{ww} \rangle = \frac{\tau_{ww}}{\beta_{ww}} \Gamma\ (1/\beta_{ww}) \quad , \tag{3.2.5}$$

where $\Gamma(x)$ is the gamma function. The average frequency is not $1/\langle \tau_{ww} \rangle$, but is given by

$$\langle \omega_{ww} \rangle = \langle 1/\tau_{ww} \rangle = \int_0^\infty \frac{1}{\tau} \rho_{ww}(\tau)\ d\tau$$

$$= (-1) \frac{d\phi_{ww}(t)}{dt}\Big|_{t=0} \tag{3.2.6}$$

3.3 The Cole-Davidson Function

The Cole-Davidson distribution function (assuming a distribution of relaxing processes) was first introduced in 1950 and is given by

$$\rho_{CD}(\tau) = \frac{\sin \pi \beta_{CD}}{\pi \tau} \left(\frac{\tau}{\tau_{CD} - \tau} \right)^{\beta_{CD}} \qquad (3.3.1)$$

where $0 < \beta_{CD} \leq 1$ and $\rho_{CD}(\tau)$ is zero for $\tau \geq \tau_{CD}$. This distribution was originally used to empirically fit dielectric relaxation data. The relaxation function can be obtained from Eqs. (3.2.2) and (3.2.3)

$$\phi_{CD}(t) = \int_0^\infty e^{-t/\tau} \rho_{CD}(\tau) d\tau$$

$$= \Gamma(\beta_{CD}, t/\tau_{CD})/\Gamma(\beta_{CD}).^{34} \qquad (3.3.2)$$

The average relaxation time can be obtained from Eq. (3.2.4)

$$\langle \tau_{CD} \rangle \equiv \int_0^\infty \tau \rho_{CD}(\tau) d\tau$$

$$= \tau_{CD} \beta_{CD} \qquad (3.3.3)$$

3.4 Comparison

Lindsey and Patterson have recently published a detailed comparison of the Williams-Watts and the Cole-Davidson functions.[22] Two figures taken from that publication are given in Figs. 3.4.1 and 3.4.2. The first shows the two distribution functions graphed in a manner typical of that seen in dielectric relaxation publications. The values of the parameters of the two functions are given and correspond to actual experimental data from the literature. At long times the Cole-Davidson distri-

Figure 3.4.1

Comparison of the Cole-Davidson (CD) and Williams-Watts (WW) distribution functions. The β paramerers are $\beta_{CD} = 0.37$ and $\beta_{WW} = 0.50$. The τ parameters are $\tau_{CD} = 1.0$ and $\tau_{WW} = 0.25$.

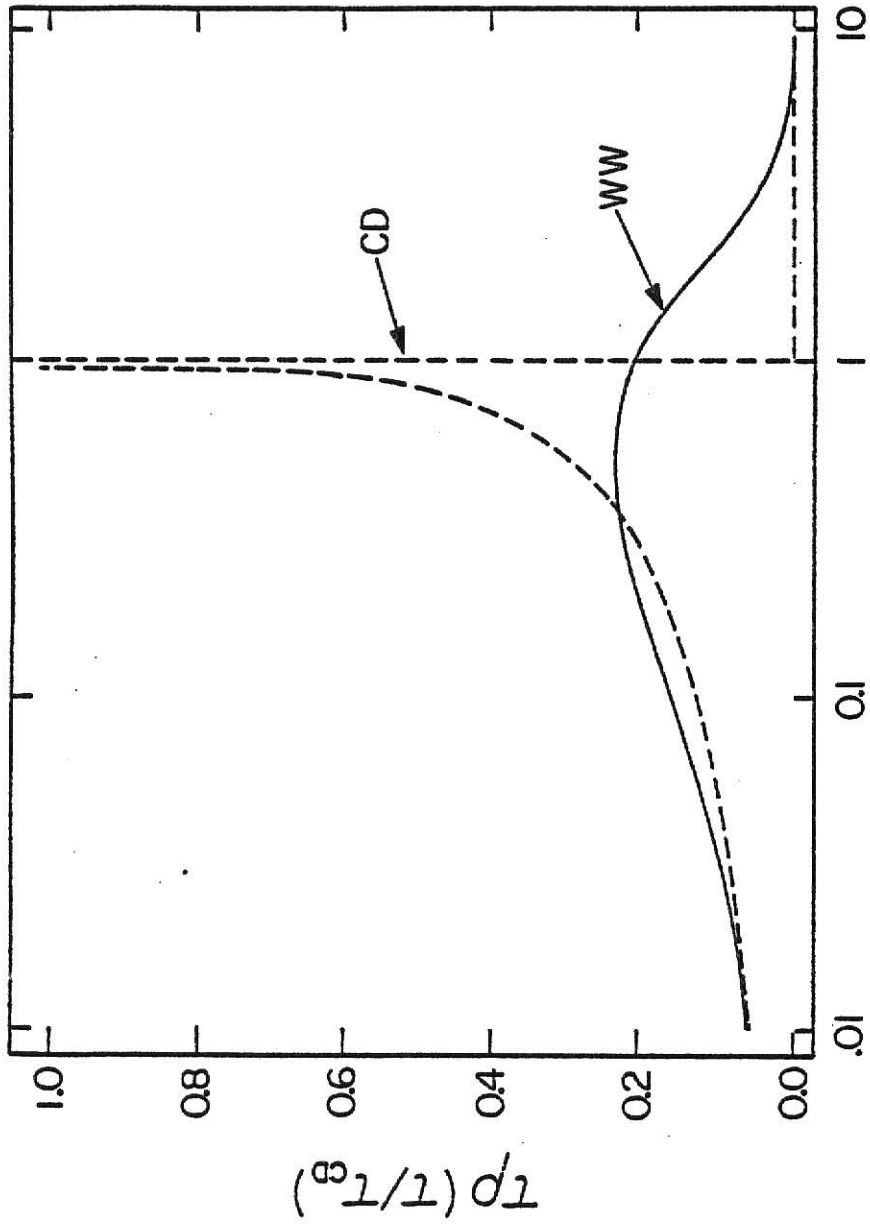
CD
WW
$\tau_p\,(\tau/\tau_{cs})$
τ/τ_{cD}
1.0
0.8
0.6
0.4
0.2
0.0
.01
0.1
10

Figure 3.4.2

Comparison of the Cole-Davidson relaxation function (dashed line) and the Williams-Watts relaxation function (solid line).

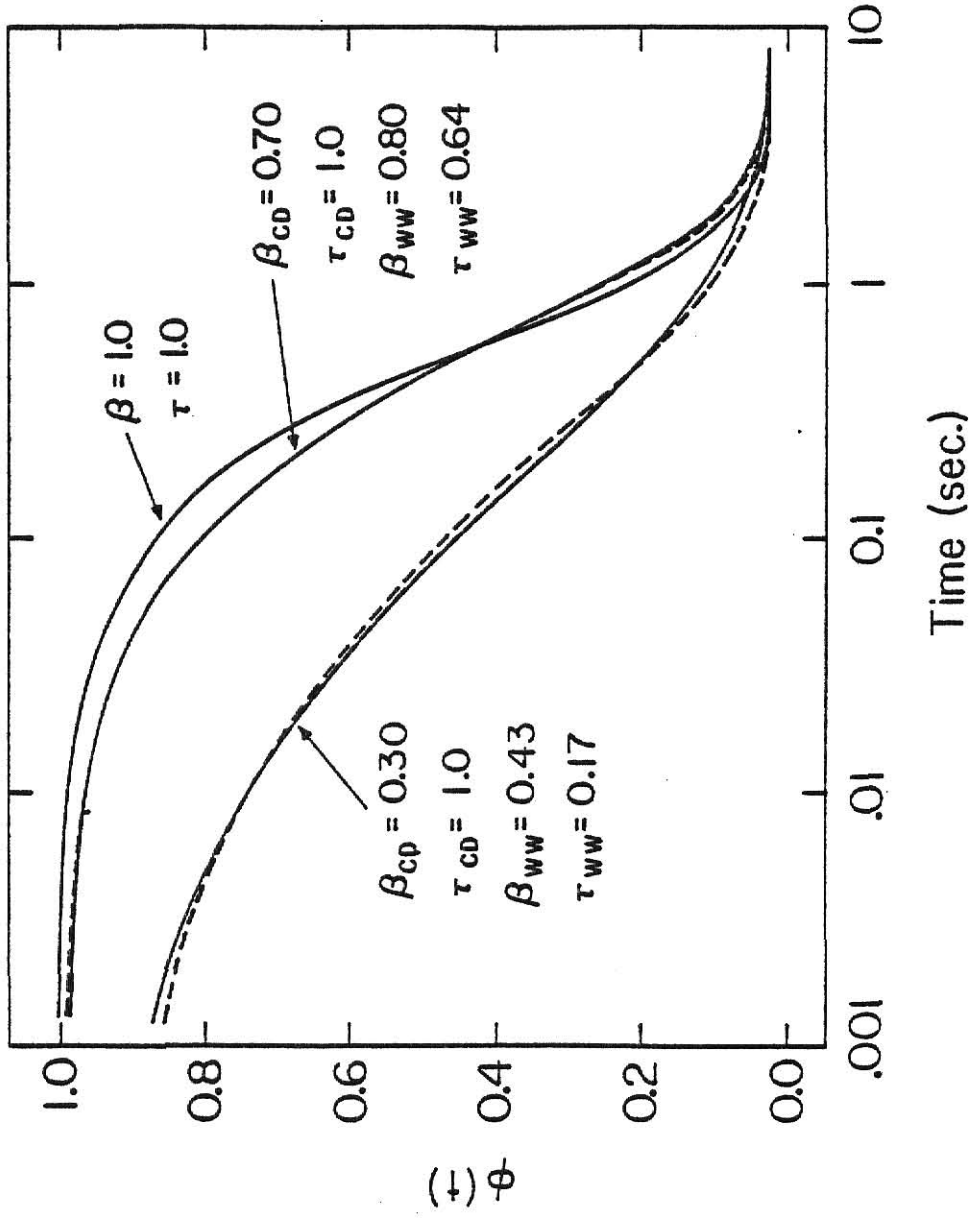
1.0
0.8
0.6
0.4
0.2
0.0
Φ (t)
.001
.01
0.1
1
10
Time (sec.)
β = 1.0
τ = 1.0
β_CD = 0.70
τ_CD = 1.0
β_WW = 0.80
τ_WW = 0.64
β_CD = 0.30
τ_CD = 1.0
β_WW = 0.43
τ_WW = 0.17

bution blows up at $\tau \approx \tau_{CD}$ and is zero for $\tau \geq \tau_{CD}$. However, the Williams-Watts function is continuous at all times and decays approximately exponential at very long times.

The relaxation functions are plotted in Fig. 3.4.2. It is seen that the two functions are very similar and would require high precision data to determine which function describes the data the best. The important thing to note, however, is that the value of the parameters needed to give similar fits are not the same. Lindsey and Patterson[22] have recently devised a numerical method in which one can compare the parameters $<\tau>$ and β obtained from data analyzed using the older Cole-Davidson function with the newer Williams-Watts functions.

It has already been pointed out that almost all photon correlation data has been fit to the Williams-Watts function. In fact, Williams and Watts discovered that for some materials, the experimental data fit their function better. In view of these facts together with the simple form of the Williams-Watts relaxation function and its physically more appealing distribution function, we have chosen to analyze our data using the newer Williams-Watts function.

Chapter IV

THE STRUCTURE AND PROPERTIES OF PMMA AS RELATED TO LIGHT SCATTERING

4.1 What is a Polymer?

Most polymers are synthetic organic compounds consisting of as many as a thousand or more covalently bonded repeat units.[35] The atoms that make up the backbone (main-chain) of the macromolecule are predominantly carbon. Frequently attached to the main-chain are molecular side-groups, the character of which determines the type of polymer. Table 4.1.1 shows a few vinyl related ($CH_2 = CHX$) monomers (repeat units) all having backbones entirely of carbon atoms.

The physical properties of polymers (e.g. toughness, the ability to crystallize, etc.) as well as relaxation behavior depend on the way in which the monomers are bonded together (Fig. 4.4.1b). The monomers of most polymers are asymmetric, hence, there are several different ways in which the main-chain can be formed. For example, if all the repeat units are bonded together in a head-to-tail fashion, the polymer is termed isotactic. If successive repeat units alternate in configuration the polymer is labeled syndiotatic. Atactic refers to a completely random arrangement.

Commercial PMMA is polymerized at high temperatures and is about 60% syndiotactic and noncrystallizable.[37] Crystallizable PMMA can be produced by polymerization at lower temperatures which produces a higher degree of

Table 4.1.1

A few vinyl related monomers.

Monomor Formula	Polymer Name
$CH_2=CH_2$	Polyethylene
$CH_2=\underset{\displaystyle CH_3}{\underset{\vert}{C}}H$	Polypropylene
$CH_2=\underset{\displaystyle Cl}{\underset{\vert}{C}}H$	Poly (vinyl chloride)
$CH_2=\underset{\displaystyle C_6H_6}{\underset{\vert}{C}}H$	Polystyrene
$CH_2=\underset{\displaystyle COOCH_3}{\underset{\vert}{C}} - CH_3$	Poly (methyl methacrylate)
$CH_2=\underset{\displaystyle COOCH_2}{\underset{\vert}{\overset{\displaystyle CH_3}{\overset{\vert}{C}}}} - CH_3$	Poly (ethyl methacrylate)

syndiotacticity. Partially crystalline isotactic PMMA can also be prepared.

4.2 The Glass Transition

One of the most interesting features of glass forming materials is the glass transition, where the viscoelastic fluid continuously transforms into a rigid glassy solid material. The transition is characterized by relaxation times that become on the order of days or more and viscosities above ~10^{13} poise.

The glass transition takes place over a narrow range of temperatures which enables us to define a somewhat arbitrary temperature called the glass temperature. The most common way to measure the glass temperature, T_g, is to observe the contraction of the volume as a function temperature in a dilatometer. Figure 4.2.1 illustrates the method. Well above T_g, the volume decreases linearly with decreasing temperature. At a constant cooling rate the liquid falls out of equilibrium just above T_g. Below T_g, the volume again decreases linearly with decreasing temperature, but this time with less slope. The intersection of the two extrapolated lines defines T_g. One finds that T_g is mildly dependent on the cooling rate, e.g.

$$T_g = 105^{\circ}C \text{ at } 1 \text{ deg min}^{-1}$$

$$T_g = 100^{\circ}C \text{ at } 1 \text{ deg day}^{-1}$$

in polystyrene.[38]

Another interesting feature of the glass transition is the phenomenon

Figure 4.2.1

A typical graph of the specific volume versus temperature for glass forming materials. The glass temperature T_g is defined as the temperature at which the two extrapolated lines intersect. The vertical line represents the affect of annealing at a temperature T' below T_g. Upon reheating the material the curve regions the original line above T_g.

SPECIFIC VOLUME
T'
Tg
TEMPERATURE

known as volume hysteresis.[39,40] When the glass is annealed at a constant temperature T'; the volume decreases and may reach the relaxed equilibrium glass state if the temperature is not too far below T_g (This is commonly referred to as aging). Upon reheating the material, the curve remains below the extrapolated equilibrium line only to rejoin it at a temperature higher than T_g.

There is no experimental evidence that the glass transition is a thermodynamic one. Yet thermodynamic transitions have been predicted for temperatures well below the glass transition by two competing theories of glass formation. Gibbs and DiMarzio[41-43] proposed a theory based on a potential barrier model where rotations of parts of the polymer molecules about C-C bonds are hindered by inter- and intra-molecular forces. This theory, which is strictly applicable to polymers, predicts a second-order phase transition at a temperature $T_2 < T_g$, where the configurational entropy, equal to the difference in entropy between glass and crystal, vanishes. On the other hand, the free-volume model,[44] a theory applicable to all glass forming materials, and based on the concept of free volume, predicts either a first-order transition or no transition at all.

Unfortunately, we can not verify the above predictions since the liquid at these temperatures is not in equilibrium and the time scales would be prohibitively long.

In a later section the glass transition will be discussed in more detail in the context of structural transitions.

4.3 The Arrhenius Equation

As we shall see, there are many different motions that give rise to

light scattering in PMMA. These motions can be described and relaxation times defined in terms of potential-energy barrier models of molecular motions in polymers. The basic temperature dependence can be determined with these models. One such model is discussed in brief below.

Figure 4.3.1 shows a potential energy diagram for a thermally activated process. The simplified model consists of two states A and B separated by a potential barrier of height V_o. For example, the two states A and B may be taken as two possible orientations of the ester side-group about the C-C bond linking it to the main-chain in PMMA. Thus, the reaction coordinate would be the angle of rotation about the C-C bond.

The reaction is described by a rate equation of the form [48]

$$-\frac{dC_A}{dt} = K_A C_A \quad , \tag{4.3.1}$$

where C_A is the number of molecules in state A and K_A is called the rate constant. For a molecule to move from state A to state B it would first have to acquire sufficient thermal energy to overcome the barrier. The probability that a given molecule will possess enough energy in excess of V_o is proportional to

$$e^{-V_o/K_B T} \tag{4.3.2}$$

where K_B is the Boltzmann constant and T is the absolute temperature. The rate constant can then be defined in terms of this probability as

$$K_A \equiv Ce^{-V_o/K_B T} \tag{4.3.3}$$

Figure 4.3.1

Potential energy diagram for a thermally activated process.

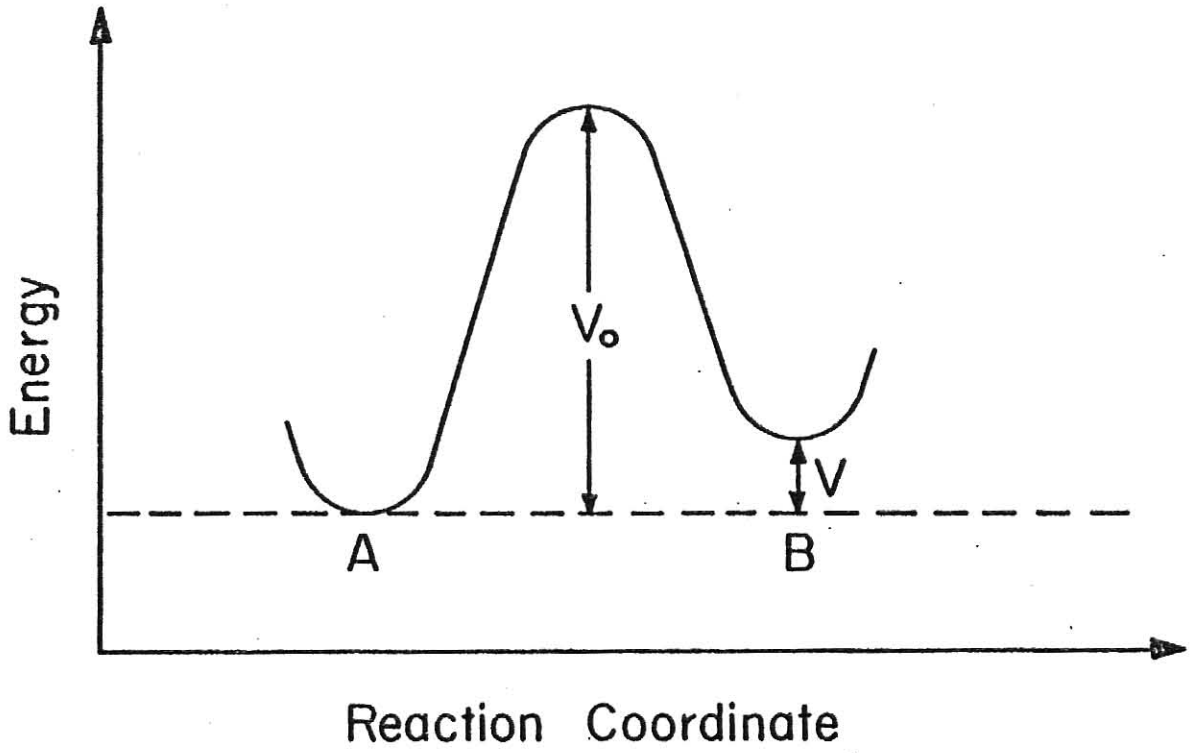
Energy
V_o
V
A
B
Reaction Coordinate

where C is a constant.

The "relaxation time" τ_c is given by[49]

$$\tau_c = 1/K_A$$

$$\tau_c = c' e^{V_o/K_B T} \quad . \tag{4.3.4}$$

This is the Arrhenius equation where V_o is the so-called activation energy. This equation has been successful in describing the temperature dependence of many relaxing processes. However, Eq. (4.3.4) breaks down near and above the glass transition. For example, a plot of $\ell n[\tau_c]$ against 1/T is curved, indicating that the activation energy is increasing as the temperature decreases (Fig. 4.4.1a). One explanation for this behavior is that the motions of the molecules, responsible for the glass transition, do not move independently of one another.[50]

An empirical equation that has been successful in describing dielectric relaxation data, near and above the glass transition in polymers, is the Williams-Landel-Ferry equation[51]

$$\ell n \frac{\tau_c}{\tau_c(T_g)} = - \frac{A(T - T_g)}{B + T - T_g} \quad , \tag{4.3.5}$$

where $\tau_c(T_g)$ is the relaxation time at the glass temperature, A and B are constants with values A ≈ 17, B ≈ 51 and are independent of the structure of the polymer.

4.4 Structural Transitions

In this section some of the intrinsic motions of the molecules that

Figure 4.4.1

Temperature dependence of the (a) α-relaxation in polyethyl acrylate and (b) β-relaxation in PMMA. (Dielectric relaxation data.)

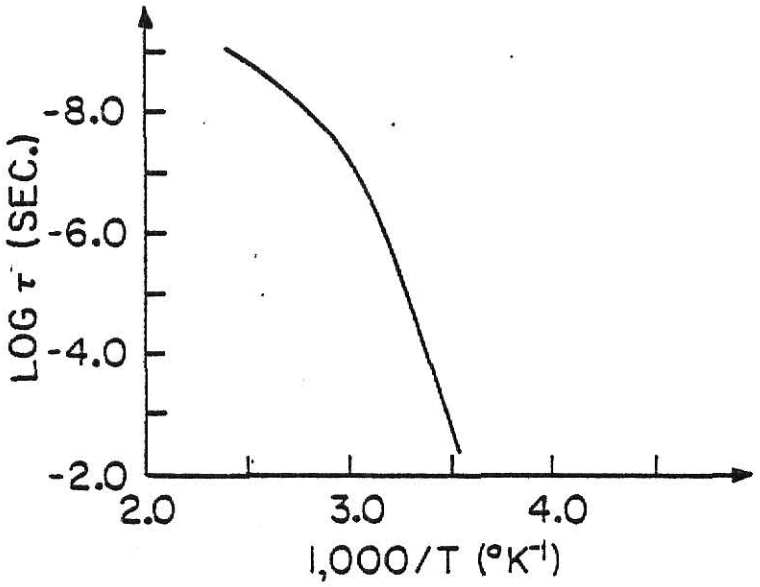
LOG τ (SEC.)
-8.0
-6.0
-4.0
-2.0
2.0
3.0
4.0
1,000/T (°K⁻¹)

(a)

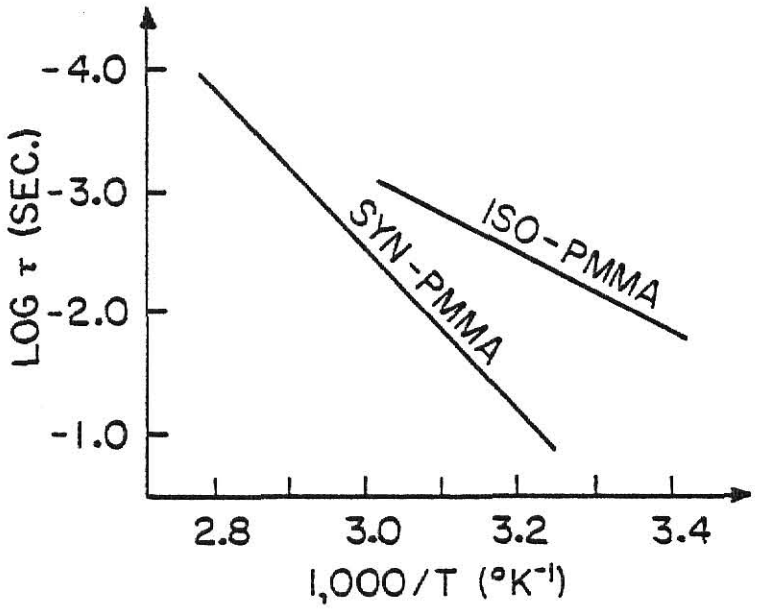
LOG τ (SEC.)
-4.0
-3.0
-2.0
-1.0
ISO-PMMA
SYN-PMMA
2.8
3.0
3.2
3.4
1,000/T (°K⁻¹)

(b)

give rise to light scattering in PMMA are identified. The freezing in or liberation of these various motions results in structural transitions from one state to another in the polymer. These structural transitions are defined and discussed as they relate to light scattering in PMMA.[52]

Structural transitions of noncrystallizable polymers can be put into two categories. First, there are transitions that result in large scale rearrangement of the structure of the polymer accompanied by the freezing in of large scale motions of large parts of the molecules. During these transitions the amorphous polymer transfers from one aggregate form into another. These large scale structural transitions are accompanied by changes in the enthalpy, heat capacity and the specific volume of the polymer (Fig. 4.4.2) and are very sensitive to thermal pretreatments. The relaxation times do not obey the Arrhenius equation (Fig. 4.4.1a).

Secondly, there are transitions involving the freezing in of local motions of the molecules such as rotations of side-groups and local motions of the main-chain. These local transitions do not involve large scale rearrangement of the polymer structure and no appreciable changes in the enthalpy and specific volume are observed. These transitions are not very sensitive to thermal pretreatment and the relaxation times obey the Arrhenius equation (Fig. 4.4.1b).

There are two large scale structural transitions in PMMA. The first occurring at about 200°C and is commonly referred to as the α' transition. As the polymer is cooled past 200°C the viscous fluid becomes a viscoelastic or rubbery substance where large-scale motions of large parts of the polymer chain become frozen in. The second large scale transition

Figure 4.4.2

Typical behavior of the (a) heat capacity and (b) enthalpy as a function of temperature near the glass temperature.

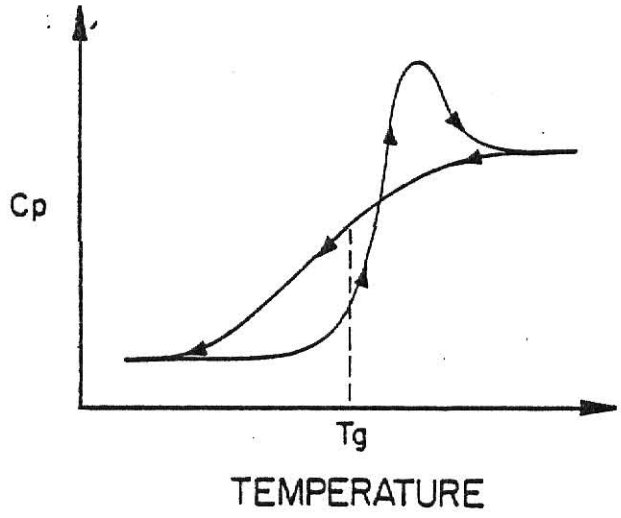

(a)

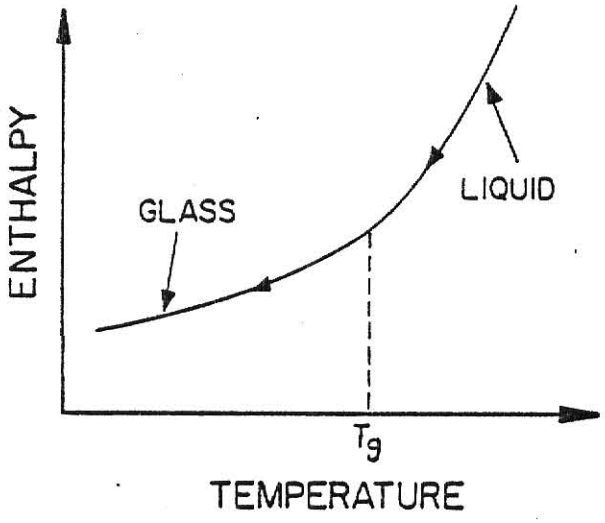

(b)

occurs at the "glass temperature" ($T_g \approx 110°C$) and is called the α transition (glass-rubber transition). Here, microbrownian motion of small molecules with 50-100 C-C bonds, together with main-chain segmental motion become frozen in at T_g. Relaxation times characterizing these motions near and above the glass temperature are commonly referred to in all polymers as the α-relaxation mode.

The first local motion transition occurs at about 30°C and is called the β transition. As the polymer is cooled past this temperature the rotation of the ester side-group about the C-C bond that links it to the main-chain and local motion of the main-chain, for example, crank-shaft-type rotation, becomes strongly hindered and eventually frozen-in. Relaxation times characterizing these motions are referred to as the β-relaxation mode. The second local motion transition is attributed to the rotation of the methyl group about the C-C bond that links it to the main-chain. This motion becomes frozen in at about -160°C and is termed the γ transition. The final local motion transition is called the δ transition and is assigned to the rotation of the methyl group attached to the ester side group. This motion is still active at temperatures as low as 4°K.

It is evident that at temperatures of interest for this experiment (30°C - 140°C), there are many different kinds of motions that would produce fluctuations in the local dielectric constant and hence give rise to light scattering. We would expect the spectrum at a given temperature to be very complex characterized by many relaxation times. Experience indicates that it is unlikely that light scattering using photon corre-

lation spectroscopy will be able to separate relaxation processes due to the different types of motions (e.g., rotation of the ester side-group). However, it is conceivable that overall motions associated with the different structural transitions (α and β processes) could be identified and separated. The inference being that the relaxation functions that describe the two processes will have sufficiently different average relaxation times and width parameters to enable their separation.

4.5 *Information Obtained from Photon Correlation Spectroscopy*

It is worthwhile at this point to discuss what is observed by the photon correlation technique.[53]

When the incident light is vertically polarized, the scattered light will contain isotropic and anisotropic components. The isotropic scattering in fluids and solids are due to density fluctuations. We can characterize these fluctuations in three ways. First, Brillouin scattering, the scattering of light from thermal sound waves. Second, Rayleigh scattering due to thermal-expansion fluctuations and thirdly, Rayleigh scattering due to the relaxation of the longitudinal compliance. Anisotropic scattering is due to the reorientations of groups of molecules that make up the polymer macromolecule as a whole. Anisotropic scattering can also arise from collisions between molecules.

All of the above processes will contribute to the relaxation function $\phi(t)$. However, not all of them can be detected directly using photon correlation spectroscopy. For example, dead time effects of the photomultiplier, after pulsing etc. generally limit the correlation spectroscopist to correlation times of 10^{-6} sec or longer.

Let's examine each of the above mentioned processes and determine which ones can be measured using the correlation technique.

The linewidths, Γ_B, of the shifted Brillouin peaks (20°-140°C) are of the order of 100 to 400 MHz (for 90° scattering), corresponding to correlation times ($\tau_c = \frac{1}{\Gamma_B}$) of ~$10^{-8}$ sec. These peaks are shifted by as much as 10^{10}Hz. As a result, Brillouin scattering can not be detected by the digital correlator. The half-width at half-height of the central Rayleigh peak due to thermal expansion is given by

$$\Gamma_{thermal} = Kq^2/\rho C_p \qquad (4.5.1)$$

where K is the thermal conductivity, q is the magnitude of the scattering wave vector, ρ is the density, and C_p is the specific heat at constant pressure. For a scattering angle of 90°, $1/\Gamma_{thermal}$ has values in the range of 10^{-7} sec., and is therefore undetectable by photon correlation spectroscopy. The central Rayleigh peak due to the relaxation of the longitudinal compliance should yield relaxation times that are within the range of the digital correlator.[54] Anisotropic scattering induced by collisions would result in correlation times of 10^{-13} sec which are again too short to be observed. However, scattering due to reorientations of the molecules (α and β processes), have been observed by a number of workers[56-59] and we expect to observe these processes in our experiment.

We can write the relaxation function in the following form

$$\phi(t) = \sum_i a_i e^{-(t/\tau_i)^{\beta_i}} \qquad (4.5.2)$$

where $\sum_i a_i = 1$. Each term in the series represents one of the processes mentioned above. Substituting $\phi(t)$ into Eqs. (3.1.1) and (3.1.2) yields (for an ideal experiment[60])

$$C_{hom}(t)-1 = \left[\sum_i a_i e^{-(t/\tau_i)^{\beta_i}}\right]^2 \qquad (4.5.3)$$

$$C_{het}(t)-1 = (0.03)\sum_i a_i e^{-(t/\tau_i)^{\beta_i}} \quad , \qquad (4.5.4)$$

where $\frac{\bar{n}_s \bar{n}_{lo}}{\bar{n}^2} = 0.03$ for $\bar{n}_{lo} = 30\ \bar{n}_s$. As we have seen, many of the processes that scatter light in polymers are too fast to be observed with the correlation technique. As a result, the measured correlation function intercepts will be less than their ideal values, that is $C_{hom}(0) - 1 < 1$ and $C_{het}(0) - 1 < .03$. This deviation from the ideal values would enable us to determine the percent of the scattered light that represents processes too fast to be measured by the correlation technique.

It is evident that heterodyne detection is the most desirable technique in terms of separating and identifying the various processes from the data. This is because the terms due to the individual processes are mixed together by the squaring terms in Eq. (4.5.3). Thus, homodyne detection does not allow for easy separation of the individual terms as does heterodyne detection.

Chapter V

THE NEED FOR FURTHER LIGHT SCATTERING STUDIES IN PMMA

5.1 Survey of Previous Light-Scattering Experiments in Polymers

Light scattering in polymers above and below the glass transition employing photon correlation spectroscopy is relatively new. The first attempt reported in the literature was by Jackson et al. in 1973.[56] The polymer used was commercial PMMA with a glass temperature of 110°C. The experiment was conducted in the heterodyne mode at a scattering angle of 90°. The local oscillator source was provided by light scattering from static imperfections within the scattering volume of the sample. They reported the observation of two distinct exponential relaxation modes, a fast and slow decay, at temperatures ranging from 20°C to 120°C. The fast decay was attributed to side-chain motion (β-process) and the slow decay to main-chain motion (α-process). Correlations were found only in the polarized spectrum.

In 1977 Cohen et al.[57] confirmed Jackson's observations in commercial PMMA. In addition they examined the angular dependence of both the fast and slow decays. Their results showed that the fast decay was independent of the scattering angle θ, and hence a nondiffusive process. This is consistent with the notion that the fast decay is the result of side-chain motions (rotations about the C-C bond). For the slow dacay, no angular dependence was found for annealed samples but for unannealed

samples, irregular results were obtained. This behavior was believed to be the result of large inhomogeneities of the structure of the polymer.

In 1979 Patterson et al.[58,60] reported the results of depolarized Rayleigh scattering in polystyrene. The sample was polymerized in their lab under extremely clean conditions. The result was a sample essentially free of elastic scattering. This enabled them to conduct the experiment in the homodyne mode.

They observed only one scattering process which they attributed to orientational fluctuations of chain units. The data fit very well to the Williams-Watts relaxation function with a width parameter (β) of approximately 0.4. The temperature studied ranged from 99°C to 130°C (T_g = 100°C) and the observed average relaxation times decreased with increasing temperature from 34 sec to ~10^{-3} sec.

Later in that same year Lee et al.[59] reported the results of the superposition of the polarized and depolarized scattering components scattered from atactic polystyrene. They confirmed Patterson et al.'s results but in addition reported the observation of a second process two orders of magnitude faster than the first. They attributed this process to the relaxational components of the compressional and shear moduli. The data for this fast process fit well to a single exponential.

In 1980 Patterson et al.[61] reported the results of photon correlation spectroscopy of Poly(ethyl methacrylate)(PEMA) near the glass transition. The temperatures studied were from 150-70°C (T_g = 65°C). Their sample was prepared by thermal polymerization from pure monomer and was free of elastic scattering. Thus, the analysis of their measurements was

carried out in the homodyne mode.

The data at all temperatures fit well to the Williams-Watts relaxation function. The width parameters from 150°C - 120°C were near 0.40. From 110°C - 70°C the width parameters gradually decreased to a value of approximately 0.16 at 70°C. This behavior was attributed to the gradual separation of the α and β relaxation modes near T_g. However, the separation was not large enough to show two distinct parts of the relaxation function as implied in the other measurements discussed above.

5.2 Discussion and Objectives

The results of photon correlation spectroscopy in PMMA reported by Jackson et al. and Cohen et al. are unique in that single exponentials were used to describe the data. On the other hand, relaxation behavior in a number of systems including other polymers have been shown to be very nonexponential. We can think of no physical reason why PMMA should exhibit such unique behavior.

In the summer of 1979, we analyzed the scattered light from the same kind of commercial PMMA rods that Cohen et al. used in their experiments. We were unable to satisfactorily resolve the data into two decaying exponentials. Further studies in other PMMA samples produced the same results. In fact the data fit very well to the Williams-Watts relaxation function instead of one or even two exponentials.

In view of the above preliminary results it was felt that further light-scattering studies in PMMA using photon correlation spectroscopy were needed.

As noted in Sec. 5.1 Lee et al. reported the separation of the α and β modes of relaxation in polystyrene. Their method of analysis is interesting and unique. We have chosen to analyze out data using this method. The method will be discussed in some detail and serious questions will be raised pertaining to the interpretation of their results.

We have three primary objectives; 1) to demonstrate that like polystyrene and PEMA, a wide distribution of relaxation times exist in PMMA, and that the data is well described by the Williams-Watts relaxation function, 2) to demonstrate that care must be taken when interpretating data that has been analyzed using Lee's method, and 3) to observe and separate the α and β processes.

Chapter VI

EXPERIMENTAL METHOD

6.1 The Experimental Setup

The incident radiation was obtained from a Coherent Radiation Model 52 argon-ion CW laser. The 488.0nm line was used with the beam vertically polarized with respect to the scattering plane.

Figure 6.1.1 shows the main components used in this experiment. The lens L_1 focused the beam into the PMMA sample. L_2 collected the light scattered at 90° and focused the image of the scattered beam one-to-one onto a 0.010 inch pinhole. The pinhole was mounted on one end of a long brass tube. The other end of the tube was connected to a combination diaphragm and telescope system. The diaphragm allowed for easy adjustment of the intensity of scattered light falling on the cathode of the detector. The telescope combined with a reflex mirror made it possible to see the scattering volume through the center of the tube.

The scattered light was detected with a ITT FW 130 photomultiplier. The PMT output was sent via an amplifier-discriminator system to a Langly-Ford 64 channel digital correlator. The contents of the correlator memory were continuously monitored via an oscilloscope display. The memory contents could also be stored on diskets of a PDP-11 computer which was used in data analysis.

The sample was made from 3/8in thick Rohm and Haas sheet Plexiglass. A square rod was cut from the sheet and turned on a lathe to form a small

Figure 6.1.1

The main components used in our light-scattering experiment.

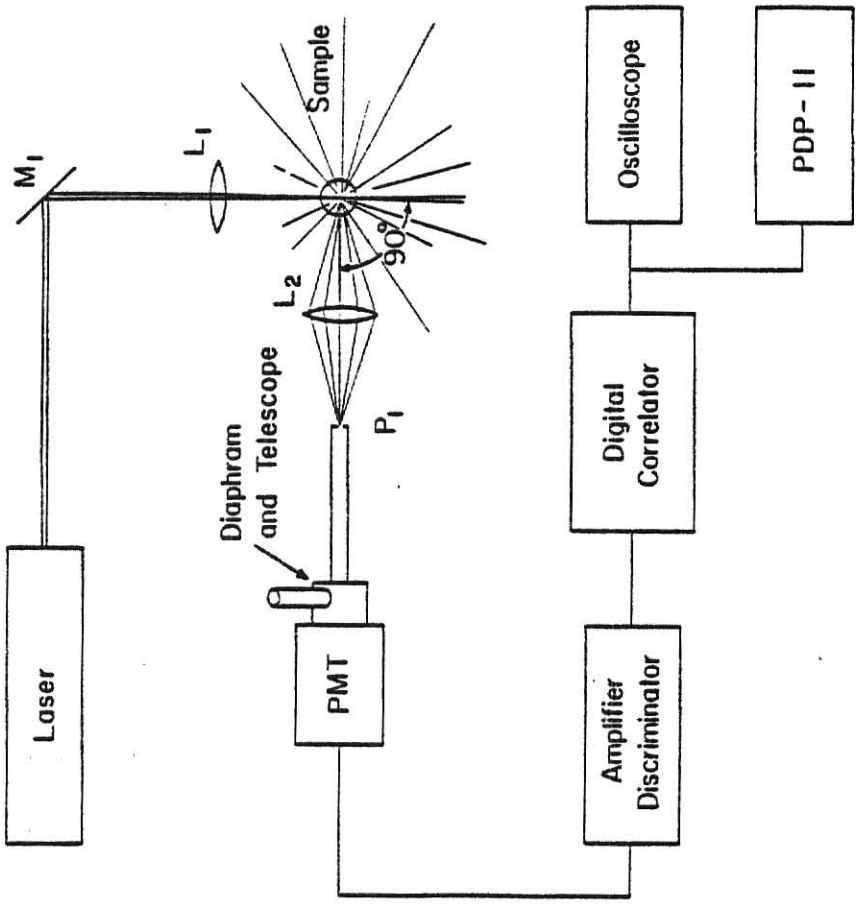
Laser
M_1
L_1
Sample
90°
L_2
P_1
Diaphram and Telescope
PMT
Amplifier Discriminator
Digital Correlator
Oscilloscope
PDP-11

cylinder rod. The sample was then polished until it became transparent.

The sample was then placed in a small test tube filled with glycerin. The glycerin was used to minimize stray light due to reflections from the various surfaces. The index of refraction of glycerin at 20°C is 1.47 and is fairly close to that of the glass (1.50) and the PMMA (1.49).

The test tube with sample was placed into a cylindrical aluminum heating cell. The cell was wrapped with mylar to provide electrical insulation for the nichrome heating wire. The cell had three small windows, two for the entrance and exit of the laser beam and one at 90° for the exit of the scattered light.

The temperature was controlled with a Cryogenic Research Company temperature controller in conjunction with a platinum resistance thermometer. The temperature stability of the system is estimated to be ~0.5°C.

The heating cell, collecting optics, and the laser were all placed on top of a Newport Research Corporation air table. The air table was necessary to eliminate building vibrations of approximately 30 Hz. The vibrations were the result of the heater and airconditioning motors that are situated in the room next to our lab.

6.2 Effects of Experimental Conditions

Before proceeding any further, it will be instructive to review the form of the unnormalized autocorrelation functions. From Eqs. (3.1.1) and (3.1.2) we have

$$G_{hom}(t) = \bar{n}^2 + \bar{n}^2\phi^2(t) \qquad (6.2.1)$$

$$G_{het}(t) = \bar{n}^2 + 2\bar{n}_{lo}\bar{n}_s\phi(t) \tag{6.2.2}$$

The correlation function data received from the digital correlator is represented in the above equations by G(t). The background term, $\bar{n}^2$, is equal to the square of the average count rate over the duration of the experiment times the duration of the experiment. The information necessary to compute the background is received from the correlator.

The data, G(t), can be put into a form that is easier to handle by first subtracting and then dividing by the background, $\bar{n}^2$, to get

$$C(t) - 1 \equiv \frac{G(t) - \bar{n}^2}{\bar{n}^2} \tag{6.2.3}$$

If we perform the same operations on the theoretical expressions (6.2.1) and (6.2.2), we get

$$C_{hom}(t) - 1 = \phi^2(t) \tag{6.2.4}$$

$$C_{het}(t) - 1 = 2\frac{\bar{n}_{lo}\bar{n}_s}{\bar{n}^2}\phi(t) \tag{6.2.5}$$

which for a Williams-Watts relaxation function become

$$C_{hom}(t) - 1 = e^{-2(t/\tau_c)^\beta} \tag{6.2.6}$$

$$C_{het}(t) - 1 = 2\frac{\bar{n}_{lo}\bar{n}_s}{\bar{n}^2}e^{-(t/\tau_c)^\beta} \tag{6.2.7}$$

The right hand side of Eqs. (6.2.6) and (6.2.7) represent the form the data would assume under ideal circumstances. In reality, however, there

are a number of experimental factors that serve to reduce correlations. In addition, several factors can produce small errors in the calculated background. As a result, the observed autocorrelation functions, for any single sample time, have the following form

$$N[C_{hom}(t) - 1] = \sigma + f(A)g(\tilde{t})e^{-2(t/\tau_c)^{\beta}} \tag{6.2.8}$$

$$N[C_{het}(t) - 1] = \sigma + 2\frac{\bar{n}_{lo}\bar{n}_{s}}{\bar{n}^2} f_h(A)g_h(\tilde{t})[B]e^{-(t/\tau_c)^{\beta}} \tag{6.2.9}$$

The new factors f, g, and B are dependent on the experimental conditions at the time of measurement and should be optimized according to the discussion contained in the following paragraphs.

Finite values of σ can arise due to systematic errors in the calculation of the background, and N is a number that facilitates the fitting of data taken at different sample times. Let's discuss each of the new factors included in the above equations.

The spatial coherence factor f(A),[62] $(1 \geq f(A) > 0)$ is a function that depends on the number of coherence areas falling on the cathode of the photomultiplier. If the scattered light is spatially coherent over the entire surface of the cathode, then photoelectrons emitted from one region of the surface will be correlated with those emitted from other regions. Under these conditions, f(A) has its maximum value of unity. On the other hand, if one region of the surface is illuminated with light that is not coherent with the light falling on other regions, averaging will occur and the value of f(A) will decrease. In the hetero-

dyne case, $f_h(A)$ behaves similarly but decreases less rapidly with decreasing coherence area than does $f(A)$.[63]

The spatial coherence factors can be theoretically calculated[64] or experimentally determined.[65] In the experiments reported in this thesis, the precise values of $f(A)$ and $f_h(A)$ are not needed. However, small values of these functions translate into small signal to noise ratios and are therefore undesirable. The number of coherence areas falling on the cathode can be reduced by decreasing the size of the pinhole placed in front of the PMT. This will, of course, reduce the detected intensity which in itself could be a problem at short sample times. With these two factors in mind, a 0.01in diameter pinhole was chosen for use.

It is known that the value of the measured correlation function is affected by the finite sample time of the digital correlator.[62] The number of pulses entering the correlator during a single sample time is proportional to the averaged scattered intensity detected during that same sample time. In view of this, it is evident that the sample time should be chosen so that it is less than the characteristic fluctuation time of the scattered light.

The functional forms of $g_h(\tilde{t})$ and $g(\tilde{t})$ have been derived for single Lorentzian spectrums.[66] The forms of these functions for a distribution of relaxation times are not presently known. However, as long as $\tilde{t} < \langle\tau\rangle$ both are expected to be approximately equal to unity.[67] Care was taken to observe this condition.

The heterodyning efficiency [B],[68] is a measure of how well the two superimposed fields are spatially matched on the detector surface. There

are three factors that would cause [B] to have values less than the theoretical maximum value of unity. 1) Angular misalignment of the two fields, 2) wavefront radius mismatch, and 3) wavefront distortion caused by the surfaces of the collecting and focusing optics.

In this experiment the local oscillator source, if any, was produced by particlates within the scattering volume. Therefore, angular misalignment and wavefront radius mismatch are not expected to contribute to reductions of [B]. To reduce the affects of wavefront distortion one should use high quality Schlieren-free lenses.

Systematic errors in the calculated background ($\bar{n}^2$) can occur for several reasons. First, long term laser intensity fluctuations and secondly, scattering processes with relaxation times long compared to the process being studied. The σ in Eqs. (6.2.8) and (6.2.9) accounts for the misnormalization caused by these sources of error. The manner in which σ is estimated from the experimental data will be discussed in the next section.

A data set taken at a single sample time covers about two decades of time. However, to adequately determine a relaxation function, with a width parameter of 0.20, six to seven decades are needed. A composite relaxation function can be produced by combining individual data sets taken at different sample times. Obviously adjacent (in time) runs should have the same correlation in the time regime where they overlap. But because of variations of the count rate and the run time, the different runs did not match but had to be adjusted by a multiplying factor we call N.

One of the scattering mechanisms contributing to the background intensity is fluorescence. We have observed that the fluorescence in PMMA decreases slowly with time after the initiation of the laser beam. This would lead to unreliable results if data was being taken during the time the fluorescence was changing.

In addition to fluorescence, the laser intensity fluctuates by approximately 15% during the first hour of operation and by about 2% thereafter.

The best procedure to follow would be to allow the laser to warm up for an hour with the beam directed through the sample. When taking data, take several runs at each sample time. In this manner inconsistant data could be recognized and discarded.

In conclusion, we did not measure the exact values of the spatial coherence factor, the heterodyne efficiency etc. As a result, the products $f(A)g(\tau)$ and $2\frac{\bar{n}_{lo}\bar{n}_S}{\bar{n}^2} f_h(A)g_h(\tau)[B]$ of Eqs. (6.2.8) and (6.2.9) are treated as adjustable parameters to give the best fit to the experimental data. Therefore, the autocorrelation functions simplify to

$$N[C_{hom}(t) - 1] = [\sigma + ae^{-2(t/\tau_c)^{\beta}}] \qquad (6.2.10)$$

$$N[C_{het}(t) - 1] = [\sigma + a_h e^{-(t/\tau_c)^{\beta}}] \qquad (6.2.11)$$

6.3 Preliminary Discussion

Several groups working independently have discovered that it is impossible to completely eliminate the particulates or inhomogeneities responsible for the elastic scattering in PMMA.[69,70] This is not true

for at least two other clear polymers that have been polymerized under extremely clean conditions. The Rayleigh-Brillouin spectrums of polystyrene and poly(ethyl methacrylate) show very low apparent Landau-Placzek ratios near T_g. This indicates that the samples are essentially free of elastic scattering. As a result the light scattering experiments in these polymers have been conducted in the homodyne mode.

It has already been pointed out that in a heterodyne experiment, the intensity of the local oscillator (elastically scattered light in this case) must be at least 30 times the intensity of the inelastically scattered light. This insures that the homodyne term in Eq. (2.3.8) can be neglected. For commercial PMMA rods the heterodyne condition is probably satisfied as indicated by the very low signal to noise ratios ($S/N < 0.02$) obtained by Jackson et al. and Cohen et al. On the other hand, our samples (taken from commercial sheet PMMA) do not produce as much elastically scattered light as do the rods. Originally, we had assumed that the amount of elastically scattered light was still sufficient to satisfy the heterodyne condition. Recent preliminary results tend to indicate that our assumption may have been incorrect. When an outside local oscillator is purposely introduced, the slope of the room temperature relaxation function at 2ms sample time decreases. This indicates a possible shift of the relaxation function to longer times. This would not occur if the heterodyne condition had been initially satisfied. These results are by no means conclusive but they do cast some doubt on the manner in which the data was analyzed and should be interpreted.

The difference in correlation times between a strictly homodyne and a strictly heterodyne experiment is given by

$$\tau_{het} = 2^{-1/\beta}\, \tau_{hom} \qquad (6.3.1)$$

Without the knowledge of the relative intensities of the elastic and inelastic scattered light, precise values of the correlation times are impossible to obtain. Due to the uncertainties in these values for the experiments reported here, the correlation times in Eq. (6.3.1) represent limiting values. The true correlation times are expected to be somewhere between these two extremes. For values of β near 0.2, this range of uncertainty can cover more than two decades of time. Thus, the combined uncertainties due to a number of other factors (such as temperature variations) are completely over-shadowed by the uncertainty in the mode in which the experiment was conducted.

Nevertheless, it will be instructive to go ahead and analyze the data as if the true mode of the experiment was known. This will enable us to examine Lee's method of analysis and to pose some interesting questions pertaining to the interpretation of their results.

Our analysis was conducted with the assumption that the data is well described by the Williams-Watts relaxation function. Using the homodyne representation, the composite data was fit to Eq. (6.2.10).

$$N[C(t) - 1] = \sigma + ae^{-2(t/\tau_c)^{\beta}} \qquad (6.3.2)$$

The following procedure was followed to determine τ_c, $\langle\tau\rangle$ and β in PMMA.

6.4 Analysis of the Data

At each temperature studied data was taken at as many as seven different sample times. A typical data set for a sample time of 20ms is shown in Fig. 6.4.1. The individual data sets from each run were matched with the aide of a computer program and a video terminal. The values of N were adjusted to achieve good agreement at the points of overlap.

The composite relaxation function $N[C(t) - 1]$ was then plotted on similog paper. A typical plot of this kind, for a temperature of 35°C is shown in Fig. 6.4.2. The values of the baseline (σ) and the intercept ($\sigma + a$) were estimated from this graph. Due to the breadth of the relaxation process, the relaxation function, at this temperature, will not reach its intercept at the shortest times studied (10μs) nor will it reach its baseline at the longest times studied (25sec). This leads to an uncertainty in the estimated values of these quantities and hence to uncertainty in the $(1/e)^2$ point (τ_c). Experience indicates that for widths parameters near 0.2, at least three decades on either side of the 1/e point are needed to determine the baseline and the intercept with an uncertainty of less than 5%. This translates into a 20% uncertainty for τ_c and 10% uncertainty for β.

The statistics of the individual data sets are also important in determining the relaxation function. A relatively large spread in the individual data points at the shortest and longest times makes it more difficult to estimate the intercept and baseline. Poor statistics also increases the uncertainty in the matching of the individual data sets.

Figure 6.4.1

A typical plot of the data as a function of time. The sample time was 20ms and the temperature was 35°C. The ordinate represents the number of correlations registered for each channel.

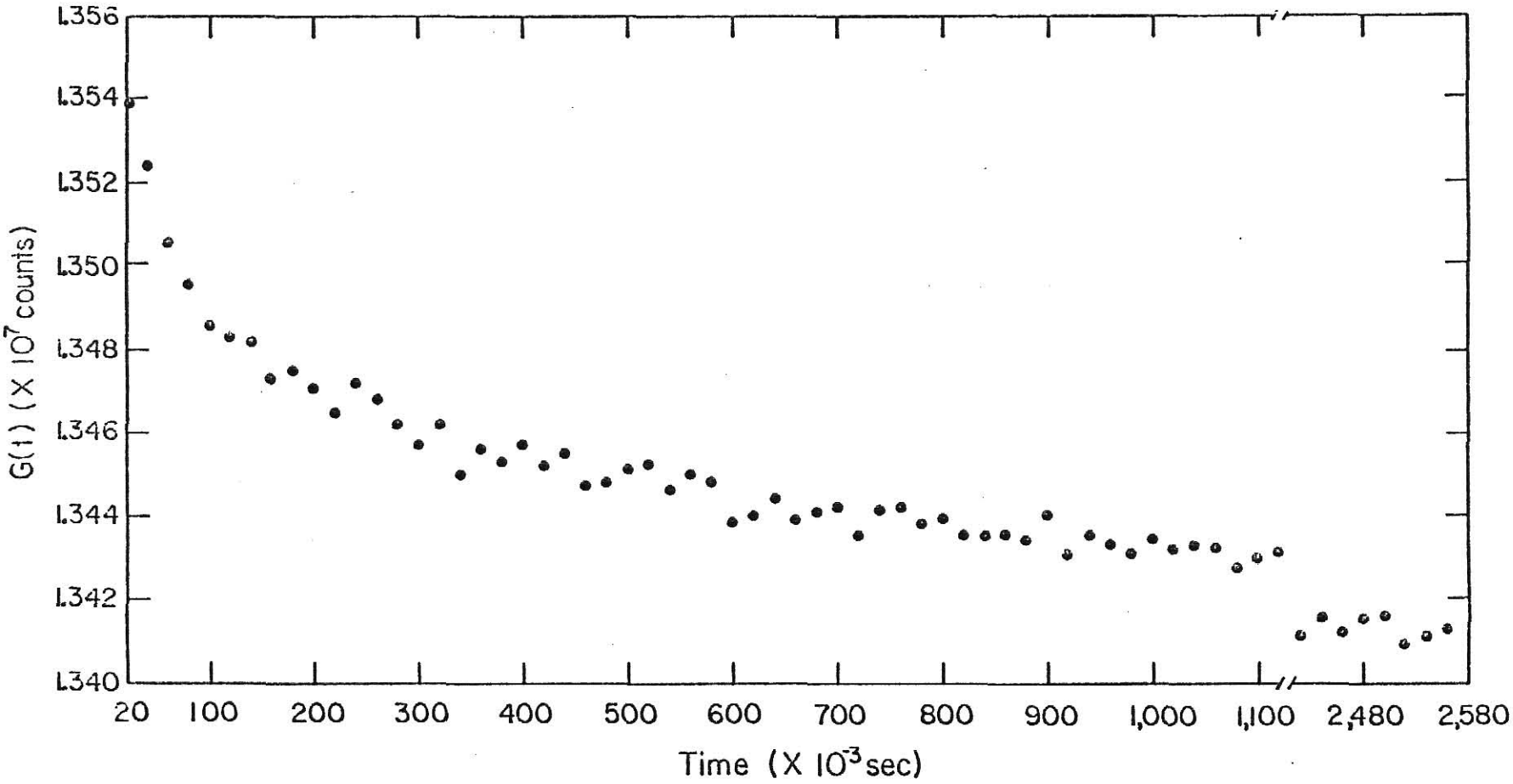
1.356
1.354
1.352
1.350
1.348
1.346
1.344
1.342
1.340
G(t) (X 10^7 counts)
20
100
200
300
400
500
600
700
800
900
1,000
1,100
2,480
2,580
Time (X 10^-3 sec)

Figure 6.4.2

The composite relaxation function N[C(t) - 1] as a function of time. Five sets of data was used at five different sample times. ● - 10μs, x - 0.2ms, ○ - 2ms, + - 20ms, and Δ - 0.5 sec. The temperature was 35°C.

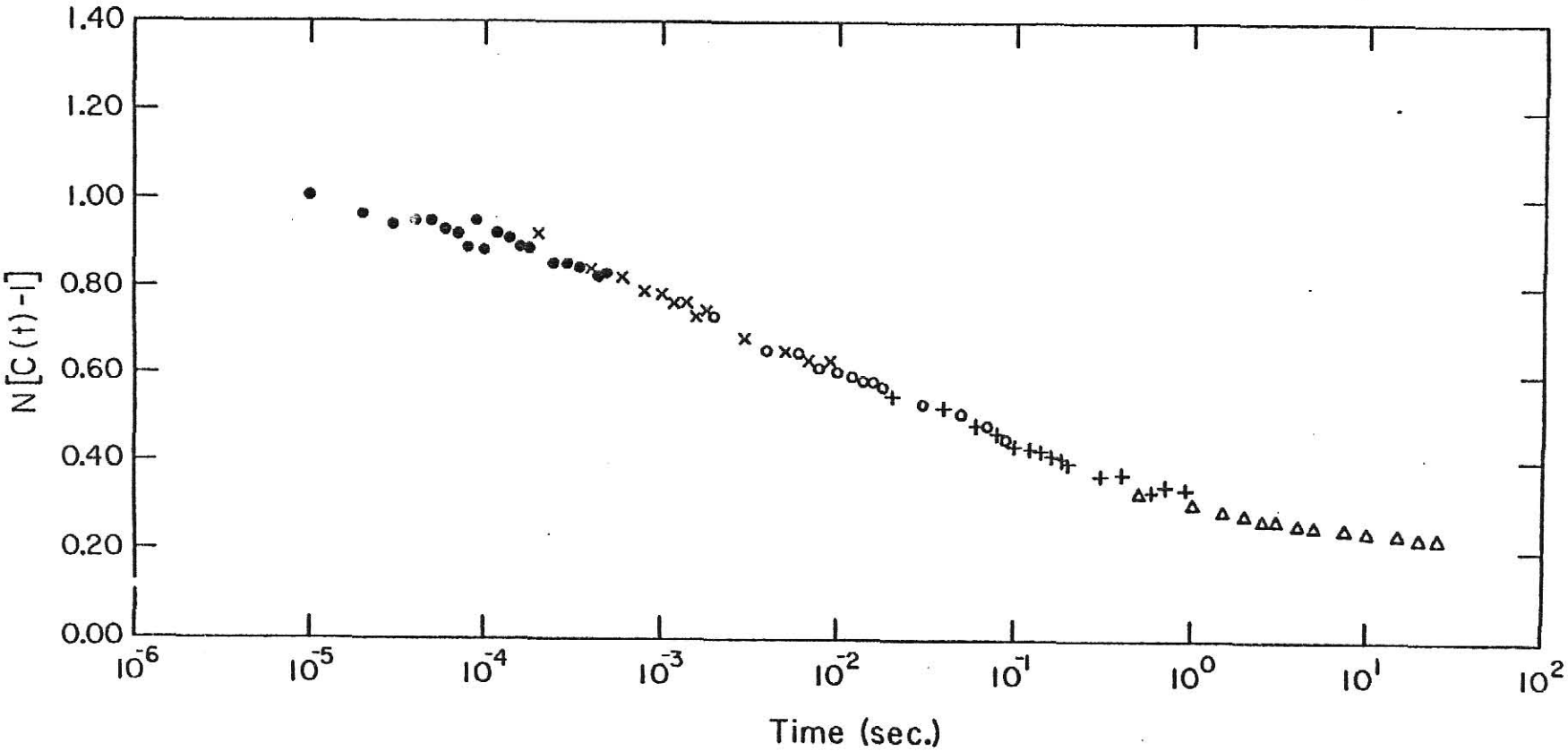
1.40
1.20
1.00
0.80
0.60
0.40
0.20
0.00
N[C(t)-1]
10^-6
10^-5
10^-4
10^-3
10^-2
10^-1
10^0
10^1
10^2
Time (sec.)

As the length of the sample time is decreased, the number of photons detected during a single sample time also decreases. Thus, long run times are needed to obtain good statistics. With the scattered intensities encountered in our experiment, run times of typically six hours or more were needed to achieve only fair statistics at a sample time of 10μs.

To determine the parameters β and τ_c, Eq. (6.3.2) was manipulated by taking the natural logarithm and then the logarithm of both sides,

$$\log\{-\frac{1}{2}\ln[\frac{N(C(t)-1)}{a}-\frac{\sigma}{a}]\} = \beta \log t - \beta \log \tau_c \quad . \quad (6.4.1)$$

On the assumption that the data fits the form of Eq. (6.3.2) a plot of the left-hand side of Eq. (6.4.1) versus the logarithm of time should yield a straight line. Curve a) of Fig. 6.4.3 shows this kind of plot for the same data of Fig. 6.4.2. (The points in Fig. 6.4.3 are not actual data points but are representative points taken from Fig. 6.4.2. Error bars on these preliminary plots are omitted for clarity.) The estimated values from Fig. 6.4.2 for σ and σ+a are 0.20 and 1.10 respectively. The plot is clearly not a straight line. Evidently the above estimated values are incorrect. The long time end of the graph can be brought into line by increasing the value of σ by 10% to 0.22. The result of this adjustment is shown in curve b) of Fig. 3.4.3. A further increase in σ by approximately 5% would lead to a noticeable "curving up" of the data at longest times.

By increasing σ+a by 9% to 1.20, the short time end of the graph can

Figure 6.4.3

A plot of $\log \{-\frac{1}{2}\ln[\frac{N[C(t) - 1]}{a} - \frac{\sigma}{a}]\}$ versus the logarithm of time. The values of σ and a are estimated from Fig. 6.4.2 a) • $\sigma = 0.20$ and $\sigma+a = 1.10$, b) x $\sigma = 0.22$ and $\sigma+a = 1.10$, and c) ○ $\sigma = 0.22$ and $\sigma+a = 1.20$.

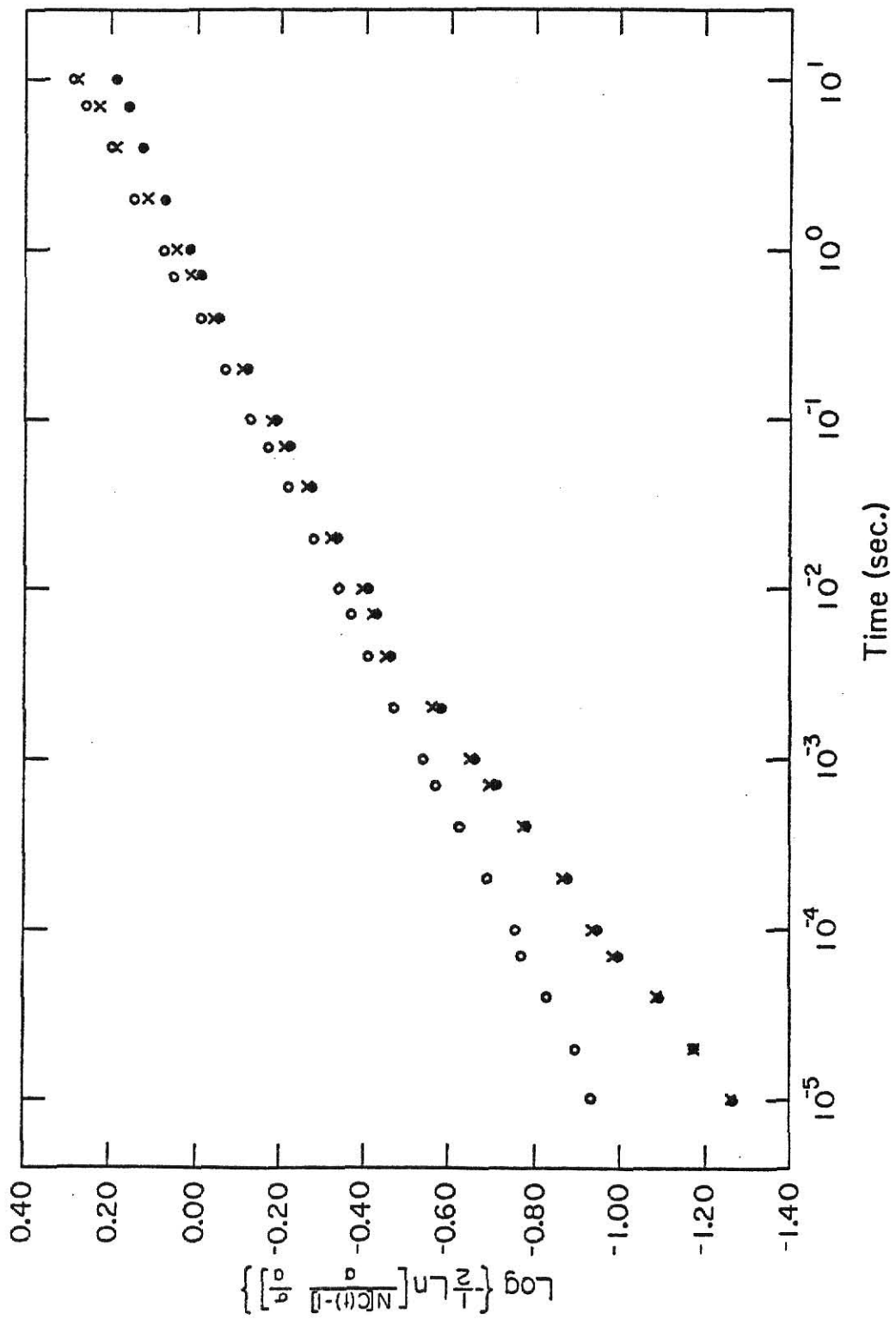
0.40
0.20
0.00
-0.20
-0.40
-0.60
-0.80
-1.00
-1.20
-1.40
10^{-5}
10^{-4}
10^{-3}
10^{-2}
10^{-1}
10^{0}
10^{1}
Time (sec.)
$\log\left\{\frac{1}{n^2}\,\mathrm{Ln}\left[\frac{N[C(t)-1]}{a}\,\frac{q}{a}\right]\right\}$

be brought in line. This is shown in curve c) of Fig. 6.4.3 and in Fig. 6.4.4 complete with error bars. Changing the value of the intercept by ±5% from this final value of 1.20 produces a noticable departure from a straight line. Thus, the data can be linearized by making reasonable adjustments in the values of the baseline and the intercept.

One of the drawbacks of this method of analysis is the distortion produced by the double logarithm at short and long times. This leads to further uncertainty in estimating the values of the intercept and baseline. The distortion becomes especially noticable when the normalized relaxation function has values higher than 0.80 and lower than 0.10. The increase in the length of the error bars at long times in Fig. 6.4.4 represent this type of distortion. The longer error bars at short times is primarily due to the poor statistics of the data taken at 10μs sample time.

Once a value for the intercept and baseline are decided upon, the values of β and τ_c can be determined from the slope and the y-intercept respectively. The dotted lines in Fig. 6.4.4 give the extreme values for the slope and y-intercept and hence give estimates of the uncertainty in β and τ_c,

The results are

$$\tau_c = 0.4 \pm 0.2 \text{ sec}$$

$$\beta = 0.21 \pm 0.02$$

It is possible to change the value of the intercept and baseline

Figure 6.4.4

A plot of log $\{ -\frac{1}{2}\ln[\frac{N[C(t) - 1]}{a} - \frac{\sigma}{a}] \}$ versus the logarithm of time. The increase in the length of the error bars at long times is due to the distortion produced by the double logarithm. The increase at short times is due primarily to the poor statistics of the 10μs data. The dotted lines give the extreme values for the slope and y-intercept.

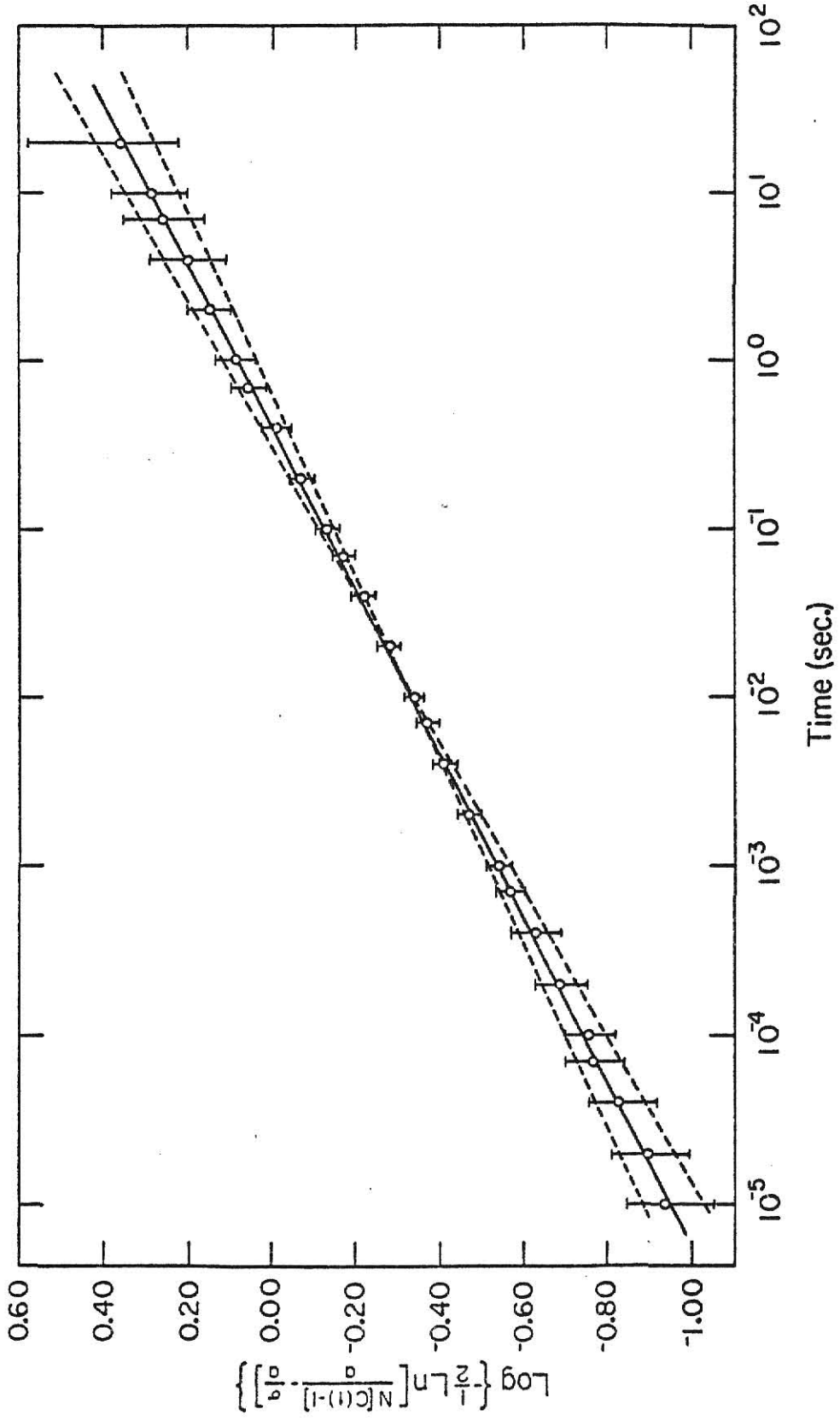
0.60
0.40
0.20
0.00
-0.20
-0.40
-0.60
-0.80
-1.00
10^{-5}
10^{-4}
10^{-3}
10^{-2}
10^{-1}
10^{0}
10^{1}
10^{2}
Time (sec.)
$\text{Log}\left\{\frac{1}{2i}\text{Ln}\left[\frac{N[C(t)-1]}{a}-\frac{a}{a}\right]\right\}$

very slightly and still obtain straight lines. But the uncertainties in β and τ_c as a result of these changes are within the uncertainties stated above.

The uncertainties produced by the $\pm 0.5^{\circ}C$ temperature variations are not expected to be significant. This is due to the expected low activation energy of the relaxation process at $35^{\circ}C$. Thus the primary source of uncertainty at this temperature is due to the relatively poor statistics of the data at short times.

The above analysis was conducted in the homodyne mode. As previously mentioned, the exact mode in which the experimental data was obtained is uncertain. If we had analyzed our data in the heterodyne mode, the correlation time, from Eq. (6.5.1), would be approximately 0.015sec. The value of β would be unchanged.

The results for temperatures above and below the glass temperature are presented in Table 6.4.5 and will be discussed further in Sec. 6.6.

6.5 Discussion

As previously mentioned, five to seven sets of data were taken at each temperature studied. Except for the data at $35^{\circ}C$ adjacent (in time) runs did not always match in the time regine where they overlapped. An example of this problem is illustrated in Fig. 6.5.1.

We investigated this problem at a later date by taking several sets of data at the same sample time and position in the sample. We found that about 70% of the runs were consistent with each other and overlapped smoothly. The other 30% of the runs did not match well, and furthermore, were inconsistent with each other. These difficulties were most likely

Table 6.4.5

The pertinent parameters of the data taken at various temperatures. T is the temperature in degrees celsius, τ_c is the $(1/e)^2$ point of the distribution, $\langle\tau\rangle_{Hom}$ is the average homodyne relaxation time given by Eq. (3.2.5), σ+a is the intercept, σ is the baseline, β is the width parameter, β_{avg} is the average value of the width parameter, and $\langle\tau\rangle_{avg}$ is the average homodyne relaxation time computed from Eq. (3.2.5) using β_{avg}.

T (°C)	τ_c (sec.)	$\langle\tau\rangle_{Hom}$ (sec.)	$\sigma+a$	σ	β	β_{avg}	$\langle\tau\rangle_{avg}$
30	1.5	10^5	1.50	0.06	0.11	0.15	4×10^3
35	0.4	40	1.20	0.22	0.21		10^3
40	0.6	370	1.30	0.25	0.17		2×10^3
55	10^{-3}	10^3	1.50	0.32	0.11		10
120	5×10^{-2}	390	2.00	0.04	0.14	0.13	2×10^3
130	6×10^{-5}	7	5.00	0.21	0.12		2

Figure 6.5.1

Illustration showing how some of the sample time data sets did not always match smoothly in the time regime where they overlap.

N [C (t)-1]
LOG (TIME)

due to laser intensity fluctuations.

The inconsistent data sets for each temperature were discarded and the remaining sets were used to construct the composite relaxation functions.

These functions were plotted on semilog paper from which the baseline and intercept were estimated. The data was then plotted in the representation of Eq. (6.4.1). The baseline and intercept were adjusted to give the best possible straight line in a reasonable length of time. In only one case, 35°C, did sufficient data exist that allowed for easy and reliable values of the baseline and intercept to be obtained from the data. In all other cases, one or more sets of data at a given temperature had to be discarded. This usually resulted in a decrease in the time window. It has been noted previously that at least three decades of time on either side of the (1/e) point ($\beta \approx 0.20$) are needed to determine the baseline and intercept with any reasonable degree of certainty. For distributions with width parameters near 0.10 these limits will have to be extended to four or more decades, a total of more then eight decades.

To illustrate this problem, consider Fig. 6.5.2a. If the estimated value of the baseline is larger than the actual value, the data will curve upward on the long time side of a plot of $\log\{-\frac{1}{2}\ln[\frac{N[C(t) - 1]}{a} - \frac{\sigma}{a}]\}$ versus log t. In addition, if the estimated value of the intercept is larger than its true value, the data is seen to curve upward on the short time side of the graph as in Fig. 6.5.2b (dotted curve). On the other hand, under estimating these parameters will result in a downward curve of the expected line at both ends as in Fig. 6.5.2b (solid curve). By

Figure 6.5.2

A hypothetical plot of log $\{-\frac{1}{2}\ln[\frac{N[C(t) - 1]}{a} - \frac{\sigma}{a}]\}$ versus the logarithm of time. a) The chosen value of the baseline is too large and results in a curving up of the data at long times. b) If the chosen values of both the baseline and intercept are too large the data curves up at both ends of the graph (dotted curve). The data curves down at both ends if the baseline and intercept are under estimated (solid curve). c) If the time window of the experiment lies between the dotted vertical lines, adjustment in the baseline and the intercept have little affect on the data.

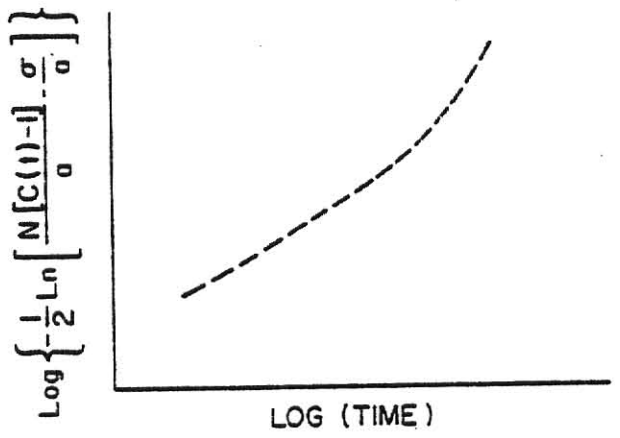
$\text{Log}\left\{-\frac{1}{2}\text{Ln}\left[\frac{N[C(t)-1]}{a}-\frac{\sigma}{a}\right]\right\}$
LOG (TIME)

(a)

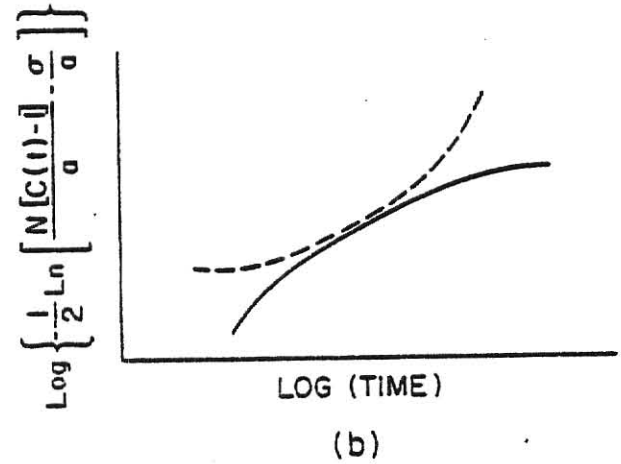
$\text{Log}\left\{-\frac{1}{2}\text{Ln}\left[\frac{N[C(t)-1]}{a}-\frac{\sigma}{a}\right]\right\}$
LOG (TIME)

(b)

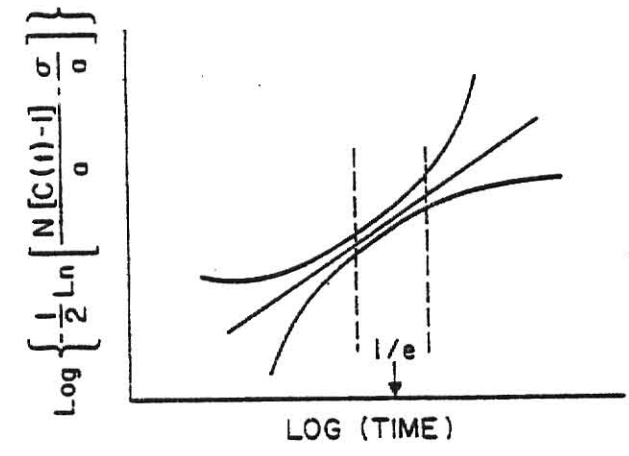
$\text{Log}\left\{-\frac{1}{2}\text{Ln}\left[\frac{N[C(t)-1]}{a}-\frac{\sigma}{a}\right]\right\}$
1/e
LOG (TIME)

(c)

appropriate adjustments of the baseline and intercept the data can be linerized. The width parameter and correlation time can then be extracted from the data according to the discussions in Sec. 6.4.

The curving of the data as described above can be seen effectively only if one has data that extends to about three decades of time either side of the 1/e point. If, for example, one has data that lie in between the vertical dotted lines in Fig. 6.5.2c any adjustments of the baseline and intercept will affect the data very little. The result is a large uncertainty for these values.

6.6 Analysis of Additional Data

At 30°C two of the five sets were discarded. The resulting time window extended from 10^{-4} sec to 6.5 sec. The data on a plot of N[C(t) - 1] versus log t, Fig. 6.6.1, showed very little change in the rate of decay over this range. The data does not display the characteristic rounding off to the intercept at short times and leveling out to the baseline at long times. Evidently, the data fall in the region of the 1/e point of the distribution. Since there was not sufficient data to adequately determine the intercept and baseline a precise value for the correlation time was impossible to obtain. The average homodyne relaxation time is in the vicinity of 10^{5} sec with a width parameter of approximately 0.11.

At 35°C five of the six sets of data were used. The time window extended from 10μs to 25 sec. Figure 6.6.2 shows that, even though there is still moderate relaxation strength at 10μs, the data appear to be

Figure 6.6.1

The composite relaxation function N[C(t) - 1] as a function of time. Three sets of data were used at three different sample times. x = 0.1 ms, + - 10 ms, and ▲ - 50 ms. The equation of the solid curves is given by Eq. (6.3.2). In all cases $\sigma = 0.06$ and $\sigma+a = 1.50$. The parameters of the curve that best fit the experimental data are $\tau_c = 1.52$ and $\beta = 0.11$. The other three curves are presented for comparison. The 1/e points were adjusted to give a convenient display. The graph shows convincingly, that there exists a wide distribution of relaxation times. The temperature was 30°C.

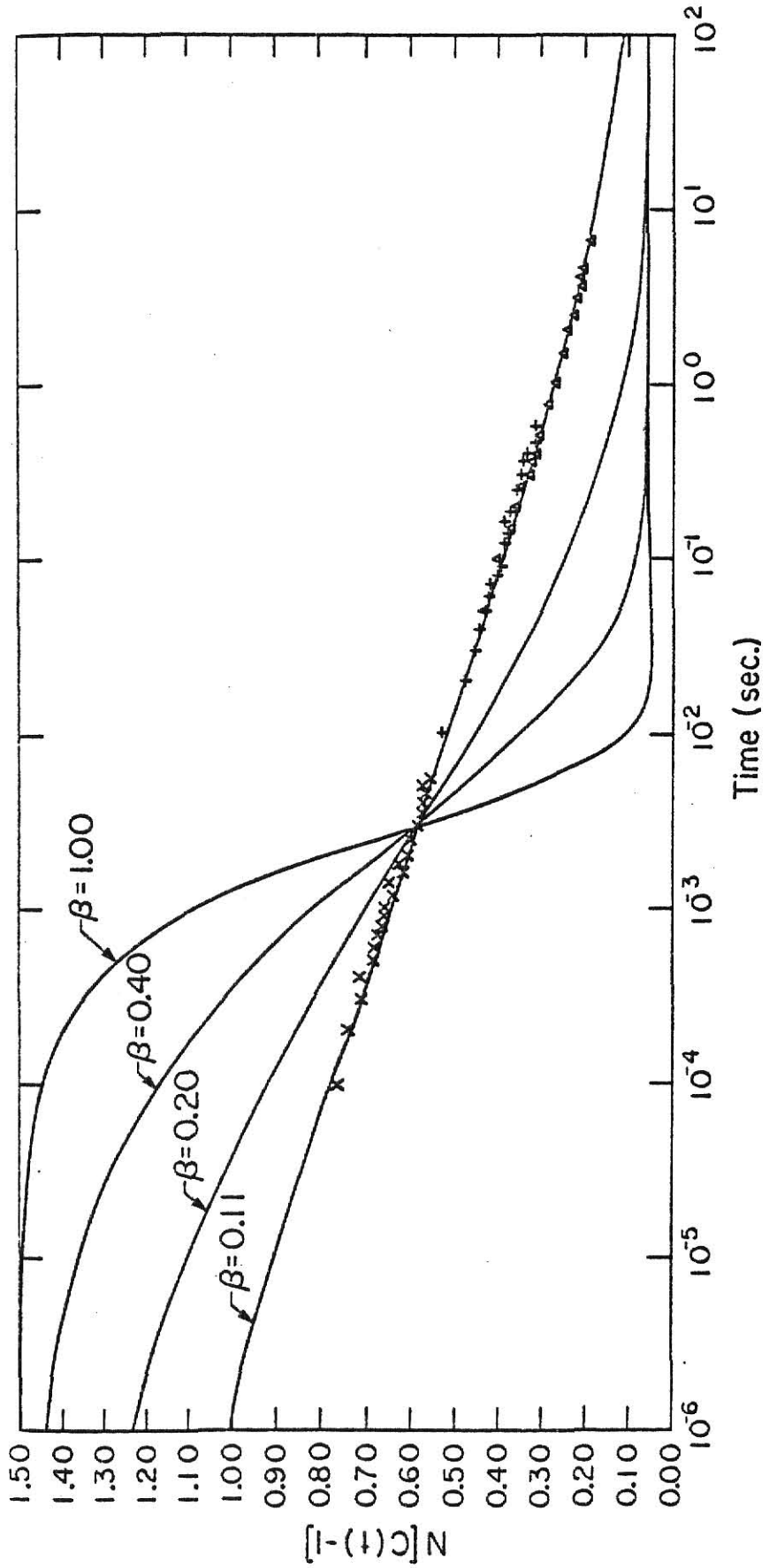
β=1.00
β=0.40
β=0.20
β=0.11
N[C(t)-C̄]
Time (sec.)
1.50
1.40
1.30
1.20
1.10
1.00
0.90
0.80
0.70
0.60
0.50
0.40
0.30
0.20
0.10
0.00
10⁻⁶
10⁻⁵
10⁻⁴
10⁻³
10⁻²
10⁻¹
10⁰
10¹
10²

Figure 6.6.2

The composite relaxation function N[C(t) - 1] as a function of time. Five sets of data were taken at five different sample times. ● - 10μs, x - 0.2 ms, o - 2 ms, + - 20 ms, and Δ - 0.5 sec. The equation for the solid curve is given by Eq. (6.3.2). $\sigma = 0.22$, $\sigma+a = 1.20$, $\tau_c = 0.4$, and $\beta = 0.21$. The temperature was 35°C.

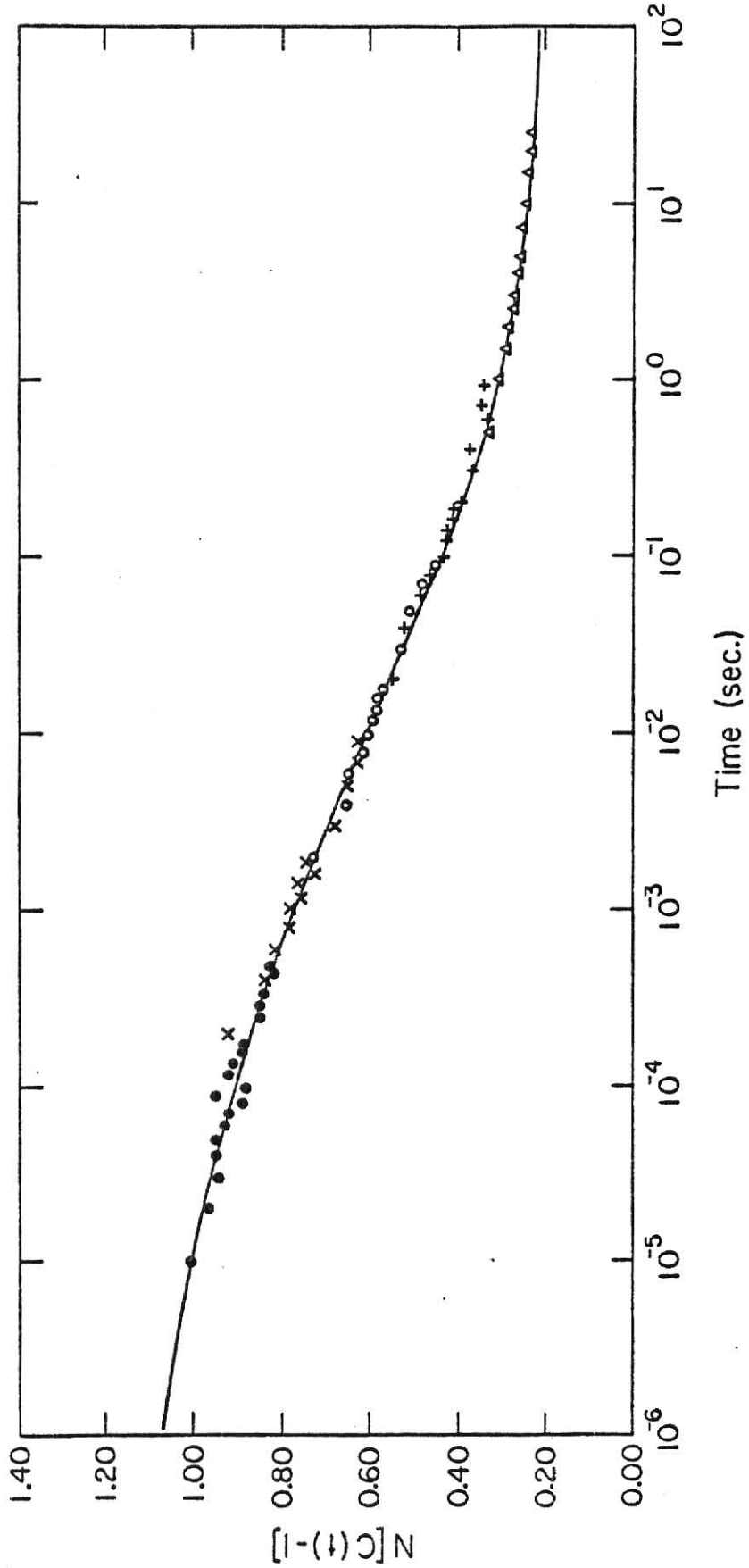
N [C(t)-1]
1.40
1.20
1.00
0.80
0.60
0.40
0.20
0.00
10^-6
10^-5
10^-4
10^-3
10^-2
10^-1
10^0
10^1
10^2
Time (sec.)

approaching the intercept. At the long time side of the graph the baseline is well defined. Very little relaxation strength remained at 10 sec.

The average relaxation time is about 40 sec and the width parameter is 0.21.

At 40°C three of the five sets of data were used. The time window extended from 10μs to 2.5sec. As can be seen from Fig. 6.6.3, the data fall near the expected 1/e point with the baseline and intercept undefined. The average relaxation time is near 370sec with a width parameter of 0.17.

At 55°C four of the five sets of data were used. The time window extended from 0.2ms to 25sec. The relaxation function had decayed to less than 5% of its maximum value by 10 ms and no noticable change could be detected past 1 sec. As Fig. 6.6.4 shows most of the data fall to the long time side of the expected 1/e point. The average relaxation time is near 10^3sec and the width parameter is 0.11.

Above the glass transition temperature ($T_g \approx 110°C$) at 120°C four of the five sets of data were used. The time window extended from 50μs to 2.5sec. Figure 6.6.5 shows that the data have begun the characteristic leveling out to the baseline by 10ms. On the other hand, there is sufficient relaxation strength at the shortest times studied to leave the intercept undefined. The average relaxation time is near 390sec and the width parameter is about 0.14.

At 130°C four of the five sets of data were used. The time window extended from 20μs to 3sec. No noticable change in decay can be observed

Figure 6.6.3

The composite relaxation function N[C(t) - 1] as a function of time. Three sets of data were used at three different sample times. • - 10μs, x - 0.1 ms, and + - 10 ms. The equation for the three curves is given by Eq. (6.3.2). Solid curve; $\sigma = 0.30$, $\sigma+a = 1.30$, $\tau_c = 0.33$, and $\beta = 0.166$. Broken curve; $\sigma = 0.25$, $\sigma+a = 1.30$, $\tau_c = 0.56$, and $\beta = 0.168$. Dotted curve; $\sigma = 0.20$, $\sigma+a = 1.30$, $\tau_c = 1.34$, and $\beta = 0.156$. At least three different curves with widely different correlation times fit the experimental data fairly well. This is an indication of the degree of uncertainty in τ_c. The temperature was 40°C.

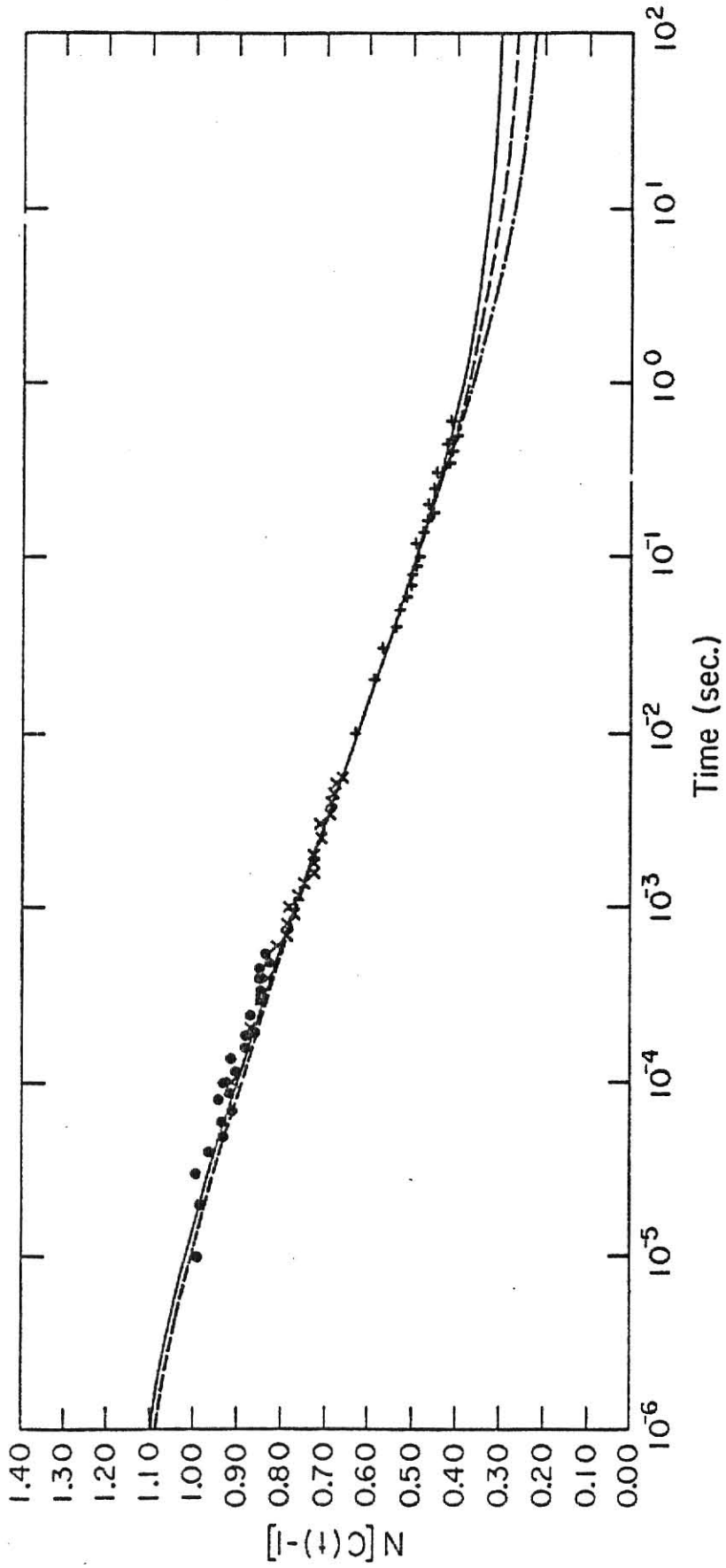
N [C(t)-1]
1.40
1.30
1.20
1.10
1.00
0.90
0.80
0.70
0.60
0.50
0.40
0.30
0.20
0.10
0.00
10^{-6}
10^{-5}
10^{-4}
10^{-3}
10^{-2}
10^{-1}
10^{0}
10^{1}
10^{2}
Time (sec.)

Figure 6.6.4

The composite relaxation function N[C(t) - 1] as a function of time. Four sets of data were used at four different sample times. ● - 20μs, x - 0.2 ms, + - 20 ms, and ▲ - 0.5 sec. The equation of the solid curve is given by Eq. (6.3.2). $\sigma = 0.32$, $\sigma+a = 1.50$, $\tau_c = 1.31 \times 10^{-3}$ and $\beta = 0.111$. The temperature was 55°C.

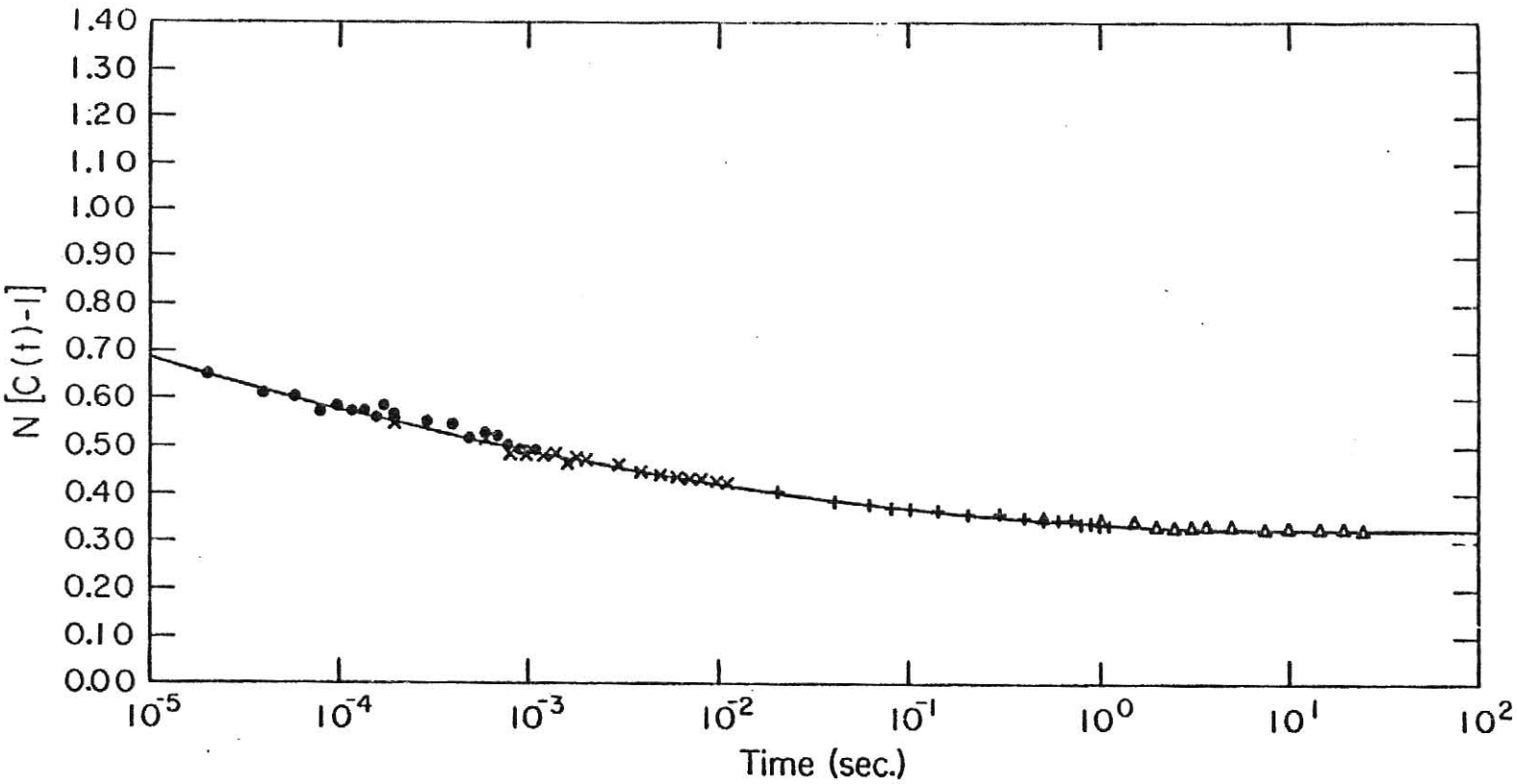
1.40
1.30
1.20
1.10
1.00
0.90
0.80
0.70
0.60
0.50
0.40
0.30
0.20
0.10
0.00
N [C (t)-1]
10-5
10-4
10-3
10-2
10-1
100
101
102
Time (sec.)

Figure 6.6.5

The composite relaxation function $N[C(t) - 1]$ as a function of time. Four sets of data were used at four different sample times. ● - 50μs, x - 0.2 ms, o - 1 ms, and Δ - 50 ms. The equation of the solid curve is given by Eq. (6.3.2). $\sigma = 0.04$, $\sigma+a = 2.00$, $\tau_c = 5.07 \times 10^{-2}$, and $\beta = 0.139$. The temperature was 120°C.

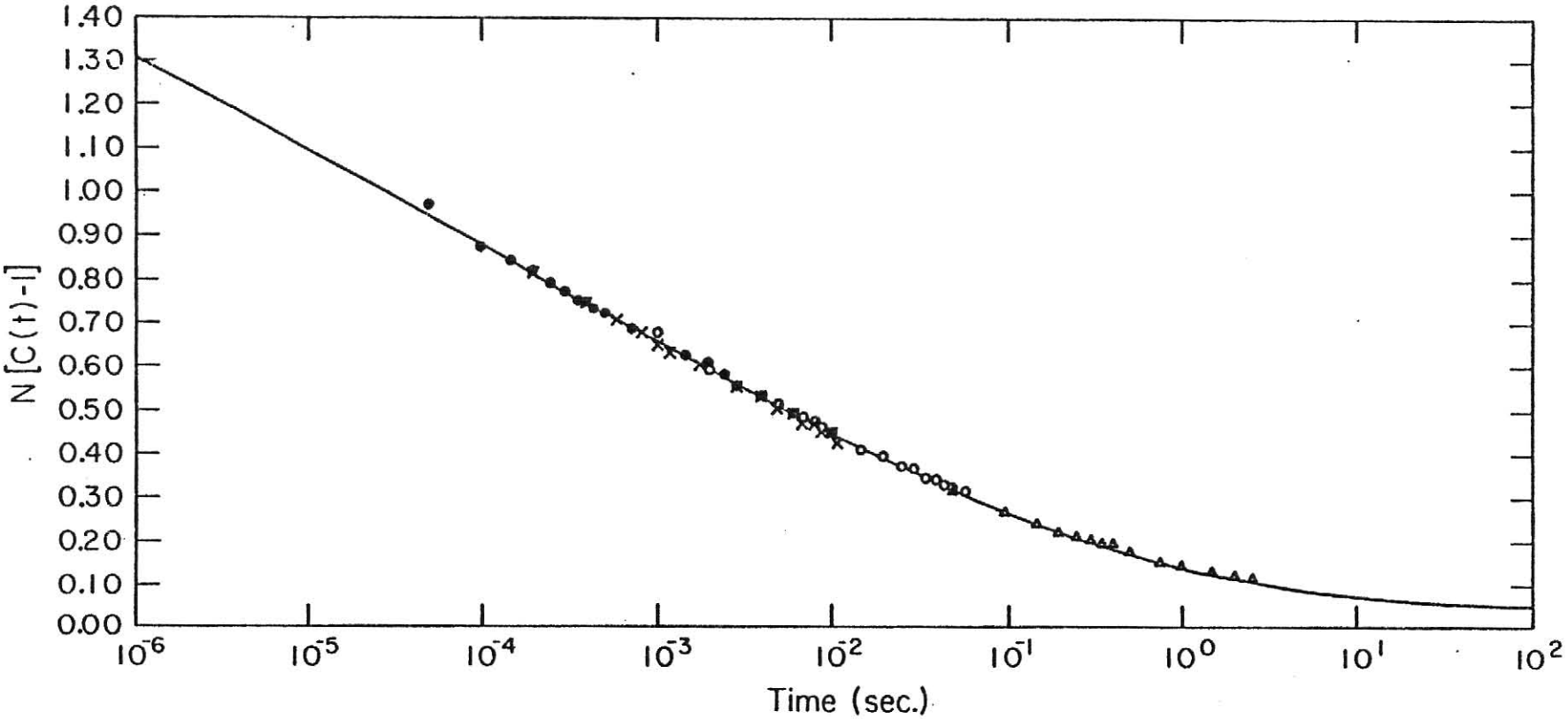
1.40
1.30
1.20
1.10
1.00
0.90
0.80
0.70
0.60
0.50
0.40
0.30
0.20
0.10
0.00
N [C(t)-1]
10^-6
10^-5
10^-4
10^-3
10^-2
10^-1
10^0
10^1
10^2
Time (sec.)

Figure 6.6.6

The composite relaxation function $N[C(t) - 1]$ as a function of time. Four sets of data were used at four different sample times. ● - 20μs, + - 0.1 ms, x - 2 ms, and * - 50 ms. The equation of the solid curve is given by Eq. (6.3.2). $\sigma = 0.21$, $\sigma+a = 4.80$, $\tau_c = 5.79 \times 10^{-5}$, and $\beta = 0.118$. The temperature was 130°C.

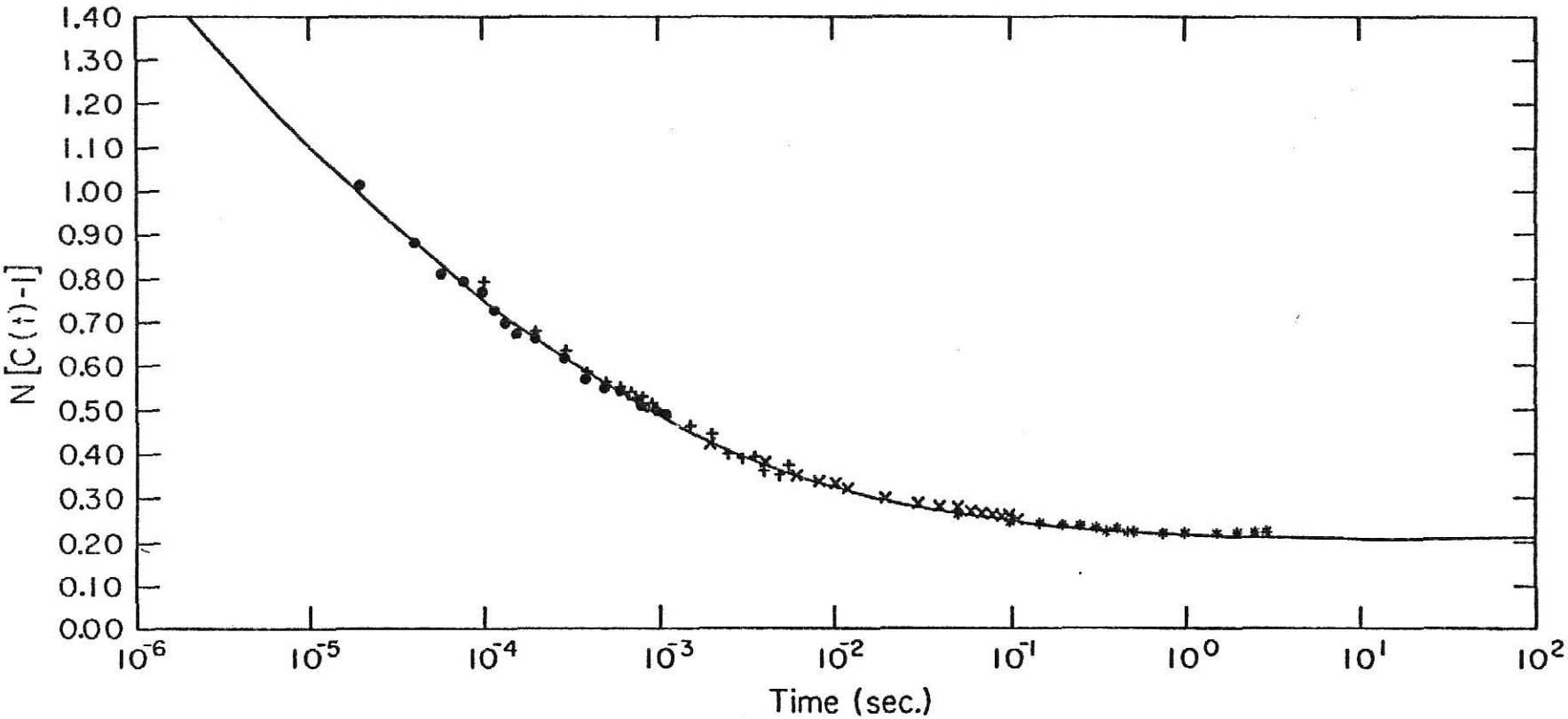
1.40
1.30
1.20
1.10
1.00
0.90
0.80
0.70
0.60
0.50
0.40
0.30
0.20
0.10
0.00
N [C(t)-1]
10⁻⁶
10⁻⁵
10⁻⁴
10⁻³
10⁻²
10⁻¹
10⁰
10¹
10²
Time (sec.)

past 0.5sec. in Fig. 6.6.6. Most of the data lie to the long time side of the 1/e point. The data show a definite shift to shorter times as compared with the 120°C data. The average relaxation times is near 7sec. The width parameter is about 0.12.

All relaxation data in the literature for polymers show that the average relaxation times for the β-process obey the Arrhenius relation. That is, as the temperature increases the average relaxation time decreases exponentially. In addition, the width parameters from correlation data have been found to be constant as long as one is not too close to the glass transition temperature. As can be seen on inspection of Table 6.4.5, our average relaxation times first decrease then increase with increasing temperature. This behavior is due to the lack of precision in the values of β. The value of β fluctuates between 0.11 and 0.21.

The average relaxation time is given by Eq. (3.2.5)

$$\langle\tau\rangle = \tau/\beta\ \Gamma\ (1/\beta) \quad . \tag{6.6.1}$$

As can be seen, $\langle\tau\rangle$ is very sensitive to fluctuations and uncertainties in β. As a result our average relaxation times are not very reliable.

In order to extract additional information from the data, we have computed an average of the existing width parameters for the temperature ranging from 30°C to 35°C. Using this average value we have computed new average relaxation times that now show Arrhenius behavior.

The Arrhenius equation is given by Eq. (4.3.4)

$$\langle\tau\rangle = C' e^{V_o/K_B T} \tag{6.6.2}$$

where V_o is the activation energy, K_B is the Boltzmann constant, T is the temperature in degrees Kelvin, and C' is a constant. Figure 6.6.7 (solid dotts) shows a plot of $\ln\langle\tau\rangle$ versus $10^3/T$ for our data. From the slope of the line the activation energy was determined using the method of least squares and found to be approximately 45 kcal/mole. This compares with about 20 kcal/mole from dielectric measurements.

Above the glass transition, polymers exhibit non Arrhanius behavior as discussed in chapter 4. A plot of $\ln\langle\tau\rangle$ versus $10^3/T$ is not a straight line but is curved indicating an increase in activation energy as the glass temperature is approached from above. Since we have only two data points in this temperature region, it is impossible to observe this behavior.

Figure 6.6.7 shows our data plotted on a graph of $\ln\langle\tau\rangle$ versus $10^3/T$. It is clear that the data taken above the glass temperature is distinct from that taken below the glass temperature. It is possible that these are two separate processes, the α-process above the glass temperature and the β-process below the glass temperature.

6.7 Data Comparison

The correlation time (τ_c) has no physical meaning. However, $\langle\tau\rangle$ is interpreted as the average relaxation time of the underlying distribution of relaxating processes. Only when there is a single relaxation process does the average relaxation time equal the correlation time.

It would be useful to know how to compare correlation spectroscopy data with relaxation data from other types of measurements. One frequently used method is dielectric relaxation. The sample is placed in an

Figure 6.6.7

A plot of $\ln\langle\tau\rangle$ versus $10^3/T$. The solid line represents a least square fit to the experimental data. The slope of the line is 2.27×10^4 and the y-intercept is -66.4. The activation energy is approximately 45 kcal/mole. ■ - The α-process above the glass transition temperature. ● - The β-process below the glass transition temperature.

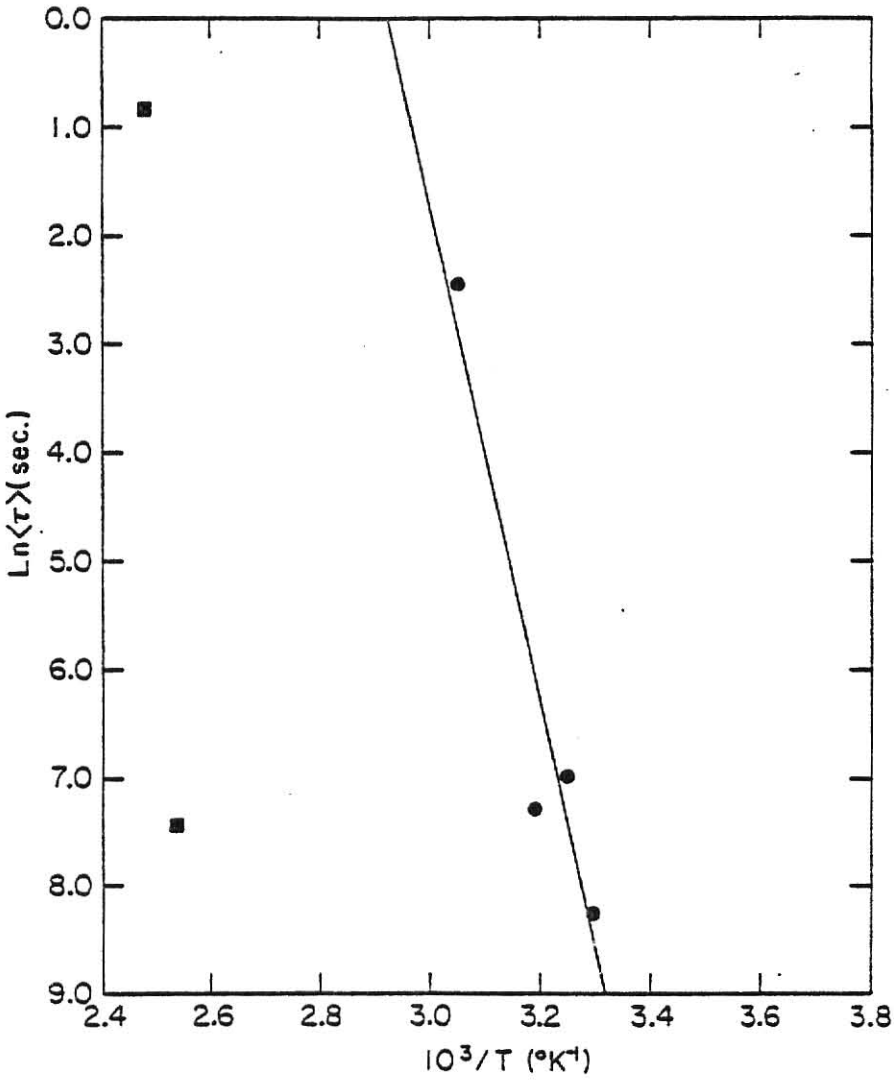
0.0
1.0
2.0
3.0
4.0
5.0
6.0
7.0
8.0
9.0
Ln⟨τ⟩(sec.)
2.4
2.6
2.8
3.0
3.2
3.4
3.6
3.8
10³/T (°K⁻¹)

oscillating electric field with angular frequency ω. The imaginary part of the complex dielectric constant, $E''(\omega)$, is measured as a function of frequency.

A semi-empirical equation purposed by Cole and Davidson that has been successful in fitting dielectric data is given by

$$E''(\omega) = E_\infty + \frac{E_s - E_\infty}{(1 + i\omega\tau_{CD})^{\beta_{CD}}} \qquad (6.7.1)$$

where E_s and E_∞ are the limiting low and high frequency dielectric constants of the sample.[71]

A graph of $E''(\omega)$ versus ω shows a maximum when $\omega\tau_{CD} = 1$. The average relaxation time is given by Eq. (3.3.3)

$$\langle\tau\rangle_{CD} = \beta_{CD}/\omega_{max} = \tau_{CD}\beta_{CD} \qquad (6.7.2)$$

The values of $\langle\tau\rangle_{CD}$ and $\langle\tau\rangle$ are the same only when $\beta_{CD} = 1.0$. For values of β_{CD} less than one, $\langle\tau\rangle$ is slightly larger than $\langle\tau\rangle_{CD}$. Empirical relationships have been devised to compare photon correlation data and dielectric data if β_{CD} is known.[72] Unfortunately, most dielectric data is presented in the form of an Arrhenius plot of log τ_{CD} (not log $\langle\tau\rangle_{CD}$) versus the logarithm of time. Furthermore, β_{CD} is not given which makes it impossible to determine $\langle\tau\rangle_{CD}$ from τ_{CD} using Eq. (6.7.2). Thus, with the exception of the activation energies, comparison of our data with dielectric data was not possible.

The Fabry-Perot interferometer can be utilized to measure the half-width at half-height of the power spectrum of the scattered light. As

mentioned previously, if the relaxation function is a single exponential decay, then the power spectrum is a Lorentzian with half-width at half-height Γ given by $1/\tau$. For a distribution of relaxation times the half-widths at half-height are smaller than would be predicted using $1/\langle\tau\rangle$. Here again, empirical relationships exist that would allow one to compare photon correlation data and power spectrum data.[73]

6.8 Discussion

The main contribution of this report is the demonstration that a distribution of relaxation times exists at all temperatures studied in PMMA. This is in contrast to the results of Jackson et al. and Cohen et al. As mentioned previously, both observed two exponentially decaying processes.

In both publications, the behavior of the correlation function at a single sample time was discussed. When the correlation function was plotted versus time it appeared as if two exponentially decaying processes were present. A fast process in front of the long tail of a slower process. We have found that when a wide distribution of relaxation times are present, the correlation functions at any sample time frequently have this same type of structure.

One must exercise caution when attempting to extract meaningful information from data taken at a single sample time. When a wide distribution of relaxation times is present, six or more decades of time will be needed to adequately determine the relaxation function. A single sample time usually covers only two decades.

As mentioned in Sec. 6.1, Lee et al. reported the observation of two separate relaxation processes in polystyrene. They were the first to introduce the idea of plotting the data in the representation of Eq. (6.4.1). Figure 6.8.1 is a reproduction of Lee et al's. data at a temperature of 111.5°C plotted in this manner. Note the striking resemblance of their plot and the plot of our data before the adjustment of the intercept (curve b) Fig. 6.4.3. Lee et al. attributed the break in the slope of their plot to the presence of two relaxation processes. The slope of the line at short times is near one indicating a single exponential. The relaxation time of 0.035sec was obtained from the y-intercept. The slope of the line at longer times is near 0.4. The correlation time obtained was 0.79×10^{-3} sec. The results from the line at long times is consistent with Patterson et al's. earlier results in polystyrene.

In the same publication the composite autocorrelation function is presented as a function of time (Fig. 6.8.2). We now make a critical test to their interpretation of the break in the linear slope of Fig. 6.8.1. Using the values they obtained for the widths parameters and correlation times, the combined relaxation functions are plotted on the same graph as the experimental data (Fig. 6.8.2 broken curve). As can be seen, the curve remains well below the experimental data up to about 10^{-2} sec. At times longer than this the curve describes the data fairly well.

It appears that the value Lee et al. choose for the intercept is too low. Figure 6.8.3 shows the results of increasing the intercept by

Figure 6.8.1

A reproduction of Lee et al's. data at a temperature of 111.5°C in polystyrene.

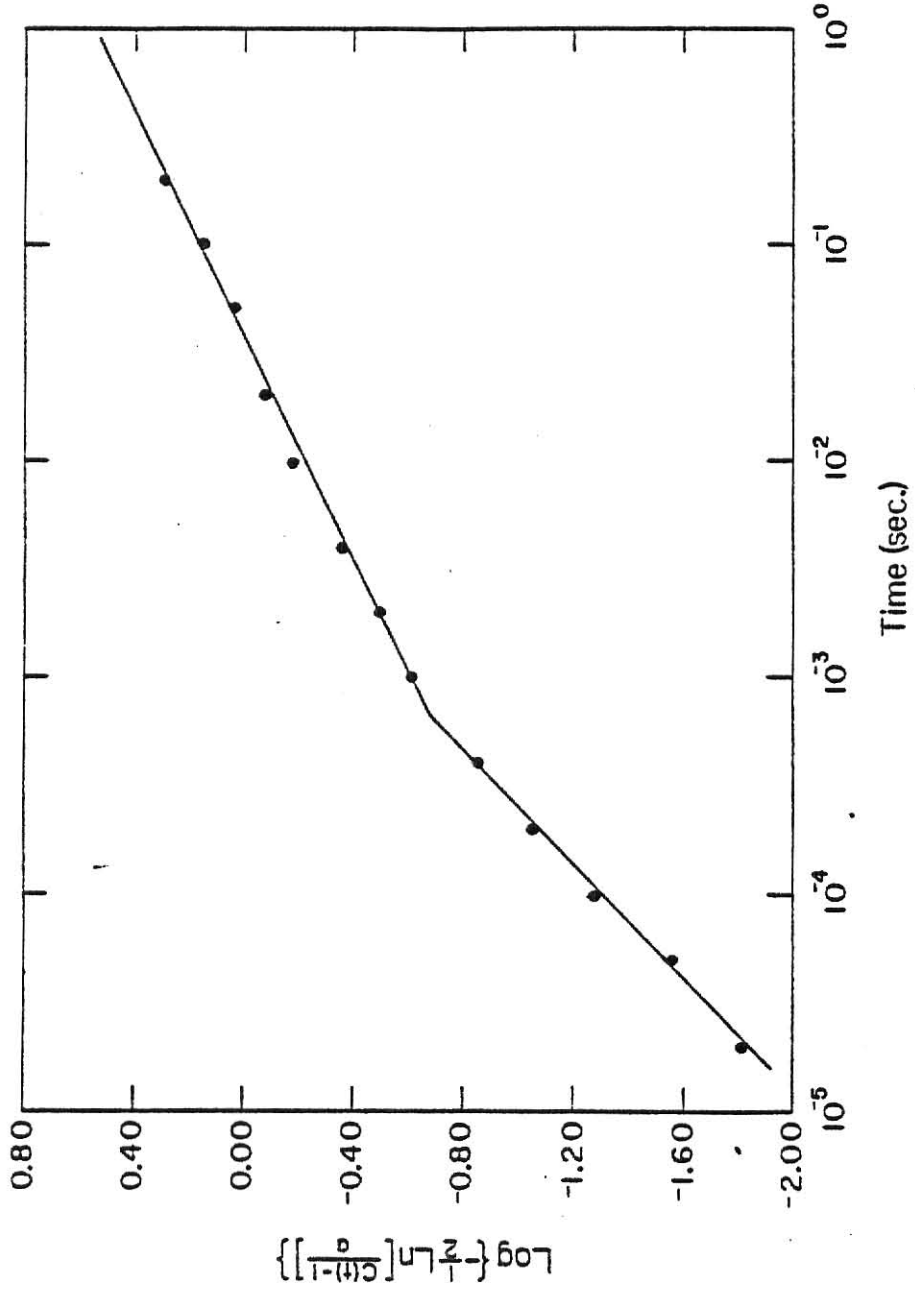
0.80
0.40
0.00
-0.40
-0.80
-1.20
-1.60
-2.00
10^{-5}
10^{-4}
10^{-3}
10^{-2}
10^{-1}
10^{0}
Time (sec.)
$\log\{-\frac{1}{2}\ln[\frac{C(t)-1}{a}]\}$

Figure 6.8.2

A reproduction of Lee et al's. data. The composite autocorrelation function as a function of time. The dotted curve represents the combined relaxation functions using the parameters reported by Lee et al. The solid curve represents the new relaxation function using the new parameters.

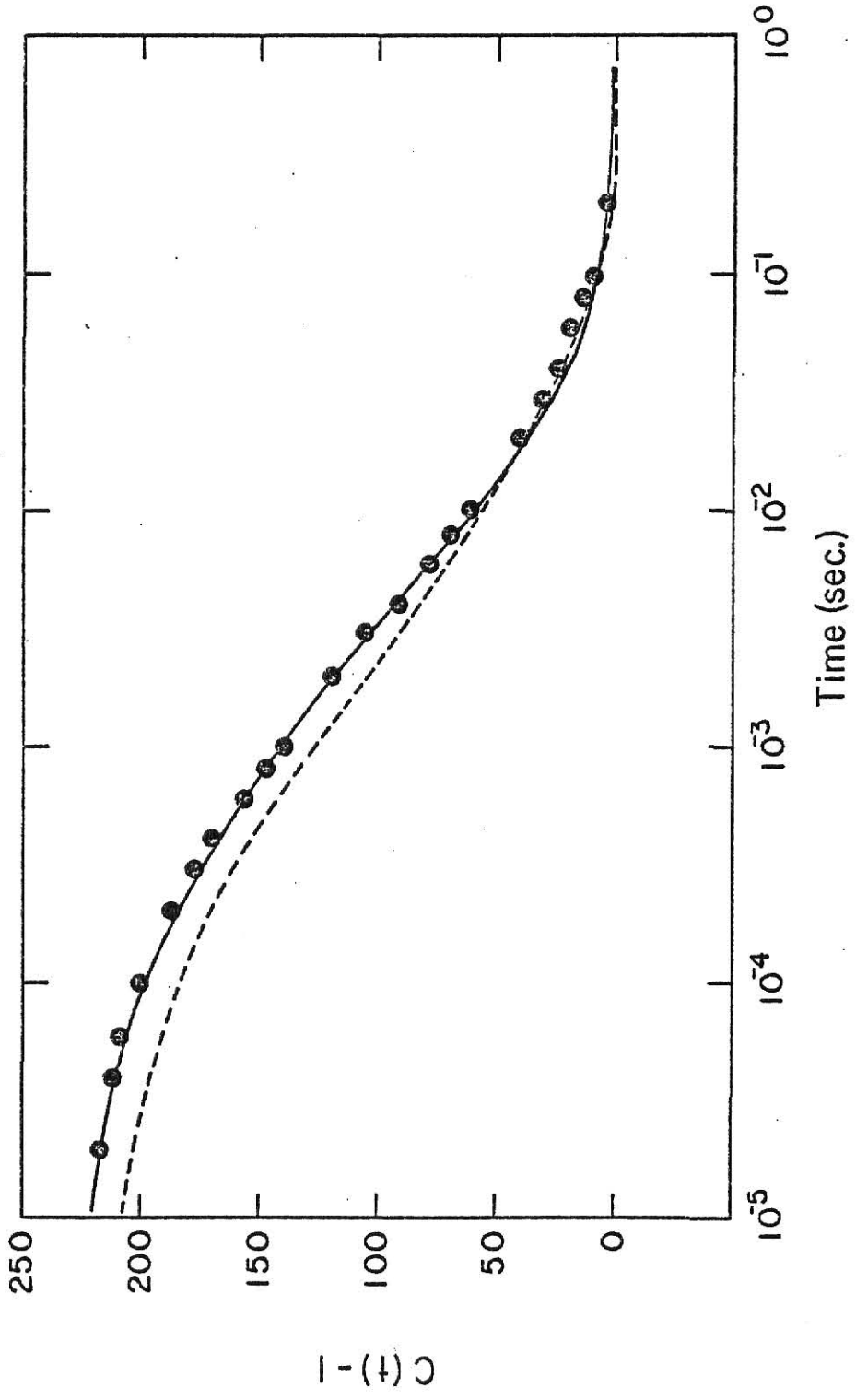
C (t) - 1
250
200
150
100
50
0
10^{-5}
10^{-4}
10^{-3}
10^{-2}
10^{-1}
10^{0}
Time (sec.)

Figure 6.8.3

A plot of Lee et al's. data after an 8% increase in the value of the intercept.

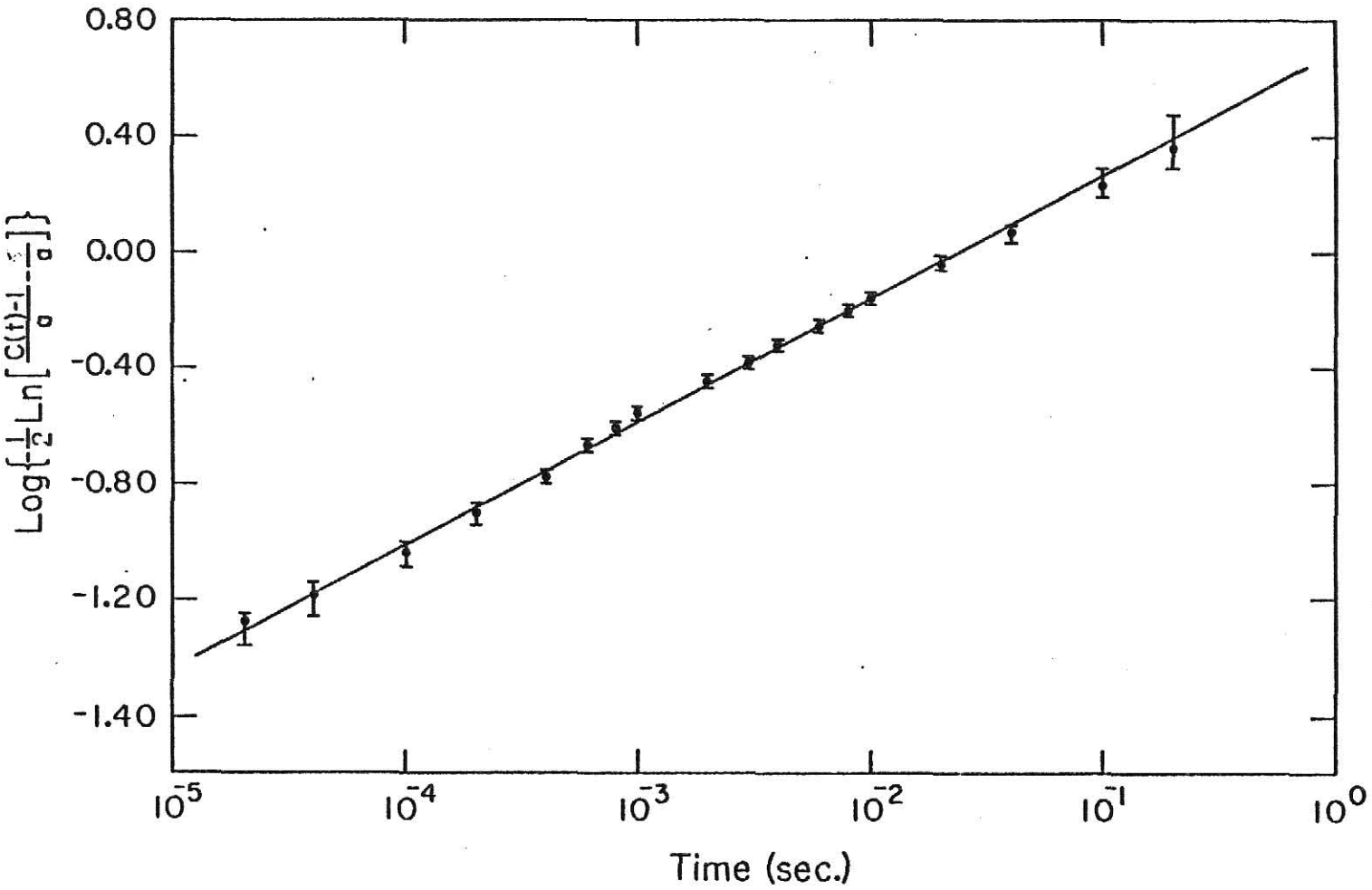
0.80
0.40
0.00
-0.40
-0.80
-1.20
-1.40
10^{-5}
10^{-4}
10^{-3}
10^{-2}
10^{-1}
10^{0}
Time (sec.)
$\mathrm{Log}\{-\frac{1}{2}\mathrm{Ln}[\frac{G(t)-1}{a}-\frac{1}{a}]\}$

8%. The data points now fit well to a single straight line. The new values of β and τ_c can then be determined in the usual manner.

The new relaxation function using the new parameters is shown on the same graph as the experimental data (Fig. 6.8.2 solid curve). As can be seen, the new relaxation function describes the data much better then the two relaxation functions that Lee et al. reported.

It appears that the break in the linear slope in Lee et al's. plot is the result of misnormalization and not to the presence of two relaxation processes.

Experience has shown that digital correlation spectroscopy is not well suited for the separation of distinct processes. This is especially true when the experiments have been conducted in the homodyne mode. However, Lee et al's. method may possibly be useful in separating relaxation processes from a heterodyne spectrum.

To test the validity of the graphical method we described in Sec. 6.4, the scattered light from 0.234μm diameter polystyrene balls in water solution was analyzed. The relaxation function for such a system is well described by a single exponential with a relaxation time of $\tau_c = (2Dq^2)^{-1}$, where D is the diffusion constant. For 90° scattering at a temperature of 20°C, $\tau_c = 4.65 \times 10^{-4}$ sec. Using the graphical method we obtained a value of 4.6×10^{-4} sec for τ_c and 1.04 for β($\beta = 1.00$ for a single exponential). Thus, the graphical method appears to be a creditable way of obtaining the pertinent parameters of the relaxation function.

Chapter VII

CONCLUSION

Photon correlation spectroscopy was used to measure average relaxation times and width parameters in PMMA. In contrast to previous experiments performed by other workers, a wide distribution of relaxation times was found at all temperatures. The width parameters below the glass temperature were near 0.15 and about 0.13 above. We were unable to separate the data, at any temperature, into two singly relaxating processes as did Cohen et al. and Jackson et al.

The Williams-Watts relaxation function was used as a fitting function. This function seemed to describe the data very well; we did not attempt to fit the data to any other function.

Below the glass temperature, the observed relaxating process was attributed to rotations of the ester side-group and local motion of the main chain. This process is commonly referred to as the β-process.

The relaxation times above the glass temperature appeared to be distinct from those below the glass temperature. This relaxating process was attributed to the α-process, microbrownian motion of small molecules and main chain segmental motion.

The activation energy for the β-process was found to be about 45 kcal/mole compared to about 20 kcal/mole as determined by dielectric measurements. The discrepancy is believed to be due to the large uncer-

tainties attached to our relaxation times and width parameters.

A graphical method, first utilized by Lee et al., was used to obtain relaxation times and width parameters. The method has several drawbacks. The data, on a plot of $\log \{-\frac{1}{2}\ln[\frac{N[C(t) - 1]}{a} - \frac{\sigma}{a}]\}$ versus $\log t$, suffers from distortion produced by the double logarithms at short and long times. In addition, many hours are needed to plot the data by hand. The best procedure would be to use a nonlinear least squares computer program to extract the desired parameters from the data.

Several factors led to large uncertainties in our results and are discussed below.

At the present time, we are uncertain as to whether the experiment was conducted in the homodyne or heterodyne mode. For width parameters near 0.15, the difference between τ_{Hom} and τ_{Het} is almost three decades of time. Before further studies are made in PMMA, this problem must be solved.

Due to laser intensity fluctuations individual data sets taken at different sample times did not always overlap smoothly. A laser intensity stablizer is a prerequisite for further light-scattering studies in polymers.

Poor statistics at short sample times made estimating the intercept difficult and increased the uncertainty in matching adjacent data. Twelve or more hours at a sample time of 1μs may be needed to achieve good statistics. Increasing the intensity of the incident laser will not solve the problem. With high laser intensities degradation of the

sample was observed after several hours.

Due to the breadth of the experimental relaxation functions, as many as three or more decades of time either side of the 1/e point may be needed to properly characterize the data. Correlation spectroscopy is limited to a time window of about 1μs to 100sec., a total of eight decades. Thus, we would expect the relaxation functions that would be the easiest to characterize would have 1/e points that fall between about 1ms and 0.1sec. This represents the mid-range of the correlation spectroscopists time window. According to our results in PMMA, the temperature range that would most likely yield meaningful results for the β-process, is between 25°C and 45°C. And for the α-process, between 120°C and 115°C.

REFERENCES AND NOTES

1. Light-beating spectroscopy is a general term used to describe spectrometers that shift the frequency of the scattered spectrum, centered at the incident frequency, to a spectrum centered at 0Hz. The light-beating technique is described in Sec. 1.2. Photon correlation spectroscopy utilizes the light-beating technique to compute an approximation of the photon correlation function. This will be discussed in a later chapter.

2. H. Z. Cummins, N. Knable, and Y. Yeh, Phys. Rev. Lett. 12, 150 (1964).

3. S. S. Alpert, Y. Yeh, and E. Lipworth, Phys. Rev. Lett. 14, 486 (1965).

4. N. C. Ford and G. B. Benedek, Phys. Rev. Lett. 15, 649 (1965).

5. J. B. Lastovka and G. B. Benedek, Phys. Rev. Lett. 17, 1039 (1966).

6. G. B. Benedek, Optical Mixing Spectroscopy with Applications to Problems in Physics, Chemistry, Biology, and Engineering, (Presses Universitaire de France, Paris, 1968), p. 49.

7. H. Z. Cummins, "Laser Light Scattering Spectroscopy," in: Intern. School of Physics "Enrico Fermi XLII Course, Varenna, ed. R. Glauber (Academic Press, New York, 1967).

8. H. Z. Cummins and H. L. Swinney, "Light Beating Spectroscopy," in Progress in Optics, ed. E. Wolf (North-Holland Publishing Company, Amsterdam, 1970).

9. For a more detailed description of homodyne and heterodyne detection see reference 10 pp. 75-150 and reference 12 Chapter 4.

10. H. Z. Cummins, "Light Beating Spectroscopy" in Photon Correlation and Light Beating Spectroscopy, ed. H. Z. Cummins and E. R. Pike (Plenum Press, New York, 1974).

11. Further information on correlation functions and their properties can be found in Chapter II of reference 12.

12. B. J. Berne and R. Pecora, Dynamic Light Scattering with Applications to Chemistry, Biology, and Physics (John Wiley and Sons, Inc., New York, 1976).

13. A discussion on the statistical behavior of random processes can be found in J. Chamberlain, The Principles of Interferometric Spectroscopy (John Wiley and Sons, Inc., Chichester, 1979) p. 59.

14. B. Chu, Laser Light Scattering (Academic Press, New York, 1974) p. 49.

15. E. Jakeman, "Photon Correlation" in Photon Correlation and Light Beating Spectroscopy, ed. H. Z. Cummins and E. R. Pike, (Plenum Press, New York, 1974) pp. 86-87.

16. A single polarized component of the electromagnetic field can be represented by a scaler quantity $E(\vec{R},t)$, where $\vec{R}$ is the distance from the scattering volume to a point on the detector surface. For the time being, we will assume that the detector surface is vanishing small. Thus, the $\vec{R}$ dependence can be dropped. Spatial integration effects for real detectors will be discussed in Sec. (6.2).

17. E. Jakeman, "Photon Correlation" in Photon Correlation and Light Beating Spectroscopy, ed. H. Z. Cummins and E. R. Pike, (Plenum Press, New York, 1974) pp. 87-89.

18. E. Jakeman, "Photon Correlation" in Photon Correlation and Light Beating Spectroscopy, ed. H. Z. Cummins and E. R. Pike, (Plenum Press, New York, 1974) pp. 90-91.

19. The sample time, $\tilde{t}$, can be selected on the front panel of the digital correlator in a 1-2-5 sequence from 10^{-7} sec to 5×10^{-2} sec.

20. The Langly-Ford digital correlator used in this experiment has 64 channels. The last eight channels may be delayed an additional 64 sample times if desired.

21. Most of the information in this chapter was obtained from reference 22.

22. C. P. Lindsey and G. D. Patterson, J. Chem. Phys. 00, 000 (1980).

23. G. Williams, Dielectr. Relat. Mol. Processes 73, 151 (1975).

24. G. Williams and P. J. Hains, Chem. Phys. Lett. 10, 585 (1977).

25. J. A. Bucaro, H. D. Dardy, and R. D. Corsaro, J. Appl. Phys. 46, 741 (1975).

26. G. Williams, NATO Adv. Study Inst. Ser. C. Chem. Biol. Appl. Relaxation Spectroscopy 75, 515 (1975).

27. G. Williams and D. C. Watts, Trans. Faraday Soc. 66, 80 (1970).

28. G. Williams, D. C. Watts, S. B. Dev, and A. M. North, Trans. Faraday Soc. 67, 1323 (1977).

29. D. W. Davidson and R. H. Cole, J. Chem. Phys. 19, 1417 (1951).

30. D. W. Davidson, Con. J. Chem. 39, 571 (1961).

31. G. Williams, M. Cook, and P. J. Hains, J. Chem. Soc., Faraday Trans. 2, 1045 (1972).

32. A. K. Jonscher, Phys. Stat. Sol. 6, 585 (1977).

33. C. T. Moynihan and P. K. Gupta, J. Non-Crystalline Solids 29, 143 (1978).

34. $\Gamma(z) = \int_0^\infty t^{z-1}e^{-t}\,dt$ (Real part of $z > 0$) ,

$\Gamma(z,x) = \int_x^\infty t^{z-1}e^{-t}\,dt$ (Real part of $z > 0$) .

35. A. R. Blythe, Electrical Properties of Polymers (Cambridge University Press, Cambridge, 1979) p. 3.

36. A. R. Blythe, Electrical Properties of Polymers (Cambridge University Press, Cambridge, 1979) p. 5.

37. P. Hedwig, Dielectric Spectroscopy of Polymers (John Wiley and Sons, New York, 1977) p. 75.

38. A. R. Blythe, Electrical Properties of Polymers (Cambridge University Press, Cambridge, 1979) p. 48.

39. M. H. Cohen and G. S. Grest, Phys. Rev. B 20, 1077 (1979).

40. L. C. E. Struik, "Physical Aging in Amorphous Glassy Polymers" in The Glass Transition and the Nature of the Glassy State, ed. M. Goldstein and R. Simha, Annals N. Y. Academy Sci. 279, 78 (New York Academy of Sciences, New York, 1976).

41. J. Gibbs and E. A. DiMarzio, J. Chem. Phys. 28, 373, 807 (1958).

42. G. Adam and J. H. Gibbs, J. Chem. Phys. 43, 139 (1965).

43. An outline of the Gibbs-DiMarzio theory can be found in M. Goldstein," Statistical Thermodynamics of Configurational Properties" in The Glass Transition and the Nature of the Glassy State, ed. M. Goldstein and R. Simha, Annals N. Y. Academy Sci. 279, 68 (New York Academy of Sciences, New York, 1976).

44. The free-volume theory was first proposed by Williams, Landel, and Ferry and has since been revised and improved many times. References 45-47, 39 represent just a few of many papers on the subject.

45. M. L. Williams, R. F. Landel, and J. D. Ferry, J. Am. Chem. Soc. 77, 3701 (1955).

46. M. H. Cohen and D. Turnbull, J. Chem. Phys. 31, 1164 (1959).

47. D. Turnbull and M. H. Cohen, J. Chem. Phys. 52, 3038 (1971).

48. A. R. Blythe, Electrical Properties of Polymers (Cambridge University Press, Cambridge, 1979) p. 45.

49. A. R. Blythe, Electrical Properties of Polymers (Cambridge University Press, Cambridge, 1979) p. 46.

50. A. R. Blythe, Electrical Properties of Polymers (Cambridge University Press, Cambridge, 1979) p. 49.

51. P. Hedwig, Dielectric Spectroscopy of Polymers (john Wiley and Sons, New York, 1977) p. 93.

52. Most of the material covered in this section was obtained from reference 37 pp. 70-77.

53. Most of the material covered in this section was obtained from references 54 and 55.

54. C. P. Lindsey, G. D. Petterson, and J. R. Stevens, J. Poly. Sci. 17, 1547 (1979).

55. G. D. Patterson, J. Non-Crystalline Solids 31, 109 (1978).

56. D. A. Jackson, E. R. Pike, J. G. Powles, and J. M. Vaughan, J. Phy. C: Solid State Phys. 6, L55 (1973).

57. C. Cohen, V. Sangur, and C. J. Pings, J. Chem. Phys. 67, 1436 (1977).

58. G. D. Patterson, C. P. Lindsey, and J. R. Stevens, J. Chem. Phys. 70, 643 (1979).

59. H. Lee, A. M. Jamieson, and R. Simha, Macromolecules 12, 329 (1979).

60. C. P. Lindsey, G. D. Patterson, and J. R. Stevens, J. Polymer Sci. 17, 1547 (1979).

61. G. D. Patterson, J. R. Stevens, and C. P. Lindsey, J. Macromol. Sci. 17, 1547 (1979).

62. E. Jakeman, "Photon Correlation" in Photon Correlation and Light Beating Spectroscopy, ed. H. Z. Cummins and E. R. Pike, (Plenum Press, New York, 1974) pp. 105-113.

63. E. Jakeman, "Photon Correlation" in Photon Correlation and Light Beating Spectroscopy, ed. H. Z. Cummins and E. R. Pike, (Plenum Press, New York, 1974) p. 112.

64. E. Jakeman, "Photon Correlation" in Photon Correlation and Light Beating Spectroscopy, ed. H. Z. Cummins and E. R. Pike, (Plenum Press, New York, 1974) p. 112.

65. G. D. Patterson, J. R. Stevens, and C. P. Lindsey, J. Macromol. Sci. 00, 1551 (1980).

66. E. Jakeman, "Photon Correlation" in Photon Correlation and Light Beating Spectroscopy, ed. H. Z. Cummins and E. R. Pike, (Plenum Press, New York, 1974) p. 106.

67. G. D. Patterson, J. R. Stevens, and C. P. Lindsey, J. Macromol. Sci. 00, 1551.

68. J. B. Lastovka, Light Mixing Spectroscopy and the Spectrum of Light Scattered by Thermal Fluctuations in Liquids. Ph.D. thesis. MIT, Cambridge, Massachusetts. (1967) pp. 225-235.

69. G. D. Patterson, personal communication.

70. C. Claiborne and B. Crist, BAPS 25, 320 (1980).

71. A. R. Blythe, Electrical Properties of Polymers (Cambridge University Press, Cambridge, 1979) p. 44.

72. G. D. Patterson and C. P. Lindsey, Macromolecules 00, 000 (1980).

73. G. D. Patterson and C. P. Lindsey, Macromolecules 00, 000 (1980).

MEASUREMENTS OF THERMALLY ACTIVATED RELAXATION TIMES IN AMORPHOUS POLY(METHYL METHACRYLATE) USING PHOTON CORRELATION SPECTROSCOPY

by

GEORGE HENRY GANGWERE III

B.S., Southwest Missouri State University, 1977

AN ABSTRACT OF A MASTER'S THESIS

submitted in partial fulfillment of the

requirements for the degree

MASTER OF SCIENCE

Department of Physics

KANSAS STATE UNIVERSITY
Manhattan, Kansas

1981

ABSTRACT

Average molecular relaxation times and activation energies in Poly (methyl methacrylate)(PMMA) were measured using digital correlation spectroscopy. The average relaxation time obtained by this method is related to the half-width at half-height of the corresponding power spectrum. Measurements were made above and below the glass transition temperature (110°C). Contrary to previous light-scattering results in PMMA a wide distribution of relaxation times were found at all temperatures studied. The data were fit to the empirical Williams-Watts relaxation function. An Arrhenius plot of the data showed two distinct processes, one above and one below the glass transition temperature. The relaxation times above the glass temperature were attributed to the α-process, microbrownian motion and main-chain segmental motion. And the relaxation times below the glass temperature were attributed to rotations of the ester side-group and local motion of the main-chain.